Atmos. Chem. Phys., 13, 4145–4169, 2013
www.atmos-chem-phys.net/13/4145/2013/
doi:10.5194/acp-13-4145-2013

Atmospheric Chemistry and Physics Open Access

Long-term changes of tropospheric NO_2 over megacities derived from multiple satellite instruments

A. Hilboll, A. Richter, and J. P. Burrows

Institute of Environmental Physics, University of Bremen, P.O. Box 330 440, 28334 Bremen, Germany

Correspondence to: A. Hilboll (hilboll@iup.physik.uni-bremen.de)

Received: 24 October 2012 – Published in Atmos. Chem. Phys. Discuss.: 11 December 2012
Revised: 11 March 2013 – Accepted: 12 March 2013 – Published: 18 April 2013

Abstract. Tropospheric NO_2, a key pollutant in particular in cities, has been measured from space since the mid-1990s by the GOME, SCIAMACHY, OMI, and GOME-2 instruments. These data provide a unique global long-term dataset of tropospheric pollution. However, the observations differ in spatial resolution, local time of measurement, viewing geometry, and other details. All these factors can severely impact the retrieved NO_2 columns.

In this study, we present three ways to account for instrumental differences in trend analyses of the NO_2 columns derived from satellite measurements, while preserving the individual instruments' spatial resolutions. For combining measurements from GOME and SCIAMACHY into one consistent time series, we develop a method to explicitly account for the instruments' difference in ground pixel size ($40 \times 320\,km^2$ vs. $30 \times 60\,km^2$). This is especially important when analysing NO_2 changes over small, localised sources like, e.g. megacities. The method is based on spatial averaging of the measured earthshine spectra and extraction of a spatial pattern of the resolution effect. Furthermore, two empirical corrections, which summarise all instrumental differences by including instrument-dependent offsets in a fitted trend function, are developed. These methods are applied to data from GOME and SCIAMACHY separately, to the combined time series, and to an extended dataset comprising also GOME-2 and OMI measurements.

All approaches show consistent trends of tropospheric NO_2 for a selection of areas on both regional and city scales, for the first time allowing consistent trend analysis of the full time series at high spatial resolution. Compared to previous studies, the longer study period leads to significantly reduced uncertainties.

We show that measured tropospheric NO_2 columns have been strongly increasing over China, the Middle East, and India, with values over east-central China tripling from 1996 to 2011. All parts of the developed world, including Western Europe, the United States, and Japan, show significantly decreasing NO_2 amounts in the same time period. On a megacity level, individual trends can be as large as $+27.2 \pm 3.9\,\%\,yr^{-1}$ and $+20.7 \pm 1.9\,\%\,yr^{-1}$ in Dhaka and Baghdad, respectively, while Los Angeles shows a very strong decrease of $-6.00 \pm 0.72\,\%\,yr^{-1}$. Most megacities in China, India, and the Middle East show increasing NO_2 columns of +5 to $10\,\%\,yr^{-1}$, leading to a doubling to tripling within the study period.

1 Introduction

During the first decade of the 21st century, the fraction of the earth's population living in cities, which had been growing since the industrial revolution and the birth of the anthropocene, reached over 50 % (United Nations, Department of Economic and Social Affairs, Population Division, 2012). This development is closely related to increasing growth rates of megacities, large urban agglomerations of more than 10 000 000 inhabitants, and of conurbations generally. The resulting high traffic, energy use, and industrial production make them hotspot areas in terms of pollution (Molina and Molina, 2004).

One of the most important air pollutants in the troposphere is nitrogen dioxide (NO_2). It participates in a catalytic chain reaction producing ozone (O_3, Finlayson-Pitts and Pitts Jr., 1999, p. 266), is a key precursor of nitric acid (HNO_3, Finlayson-Pitts and Pitts Jr., 1999, pp. 269–272) and

acid deposition, and is directly hazardous to human health (World Health Organization, 2003). Its main source is the emission of nitrogen monoxide (NO) from the anthropogenic combustion of fossil fuels (Noxon, 1978); natural sources include biomass burning (Seiler and Crutzen, 1980), lightning (Noxon, 1976), and microbial activity in soils (Williams et al., 1992).

NO_2 and NO are often, through their daytime chemistry, coupled in the troposphere: NO reacts with O_3 to form NO_2, which in turn is photolysed to form NO. The sum of NO and NO_2 is termed NO_x. Tropospheric NO_x has a relatively short lifetime of several hours to a few days (Finlayson-Pitts and Pitts Jr., 1999, p. 267). As a result, NO_2 has its largest concentrations in the boundary layer close to the emission sources, making measurements of NO_2 columns well suited to infer NO_x emissions.

The strong absorption lines of the NO_2 molecule in the visible wavelength range of the spectrum facilitate the use of optical absorption spectroscopy for measuring atmospheric NO_2 abundances. Nadir viewing instruments have been deployed on satellite platforms since the mid-1990s. This has resulted in the global monitoring of NO_2 concentrations under consistent measurement conditions (Burrows et al., 2011). For measurements of tropospheric NO_2, the nadir-viewing Global Ozone Monitoring Experiment (GOME, on board ERS-2, $40 \times 320\,km^2$ ground pixel size; Burrows et al., 1999), the SCanning Imaging Absorption spectroMeter for Atmospheric CHartographY (SCIAMACHY, on board ENVISAT, $30 \times 60\,km^2$; Bovensmann et al., 1999; Burrows et al., 1995, and references therein), the Ozone Monitoring Instrument (OMI, on board AURA, $13 \times 24\,km^2$; Levelt et al., 2006), and GOME's operational meteorological successor GOME-2 (on board Metop-A[1], $40 \times 80\,km^2$; Callies et al., 2000) provide measurements of the upwelling radiance suitable for retrieval of tropospheric NO_2. These four instruments provide a continuous time series of tropospheric NO_2 measurements beginning in August 1995.

The measured spectra are often analysed using differential optical absorption spectroscopy (DOAS; Platt and Stutz, 2008), and scientific data products of tropospheric NO_2 have existed since the early 2000s (among others: Richter and Burrows, 2002; Leue et al., 2001; Martin et al., 2002; Boersma et al., 2004, 2007; Richter et al., 2005, 2011). Long-term changes in tropospheric NO_2 amounts can thus be investigated by combining measurements from several of these four instruments.

Whilst over large areas of relatively homogeneous NO_2 signals coincident GOME and SCIAMACHY observations agree very well (Richter et al., 2005), they show considerable differences for ground scenes with steep gradients in the tropospheric NO_2 columns. This is the result of spatial smoothing, which differs depending on the ground resolution of the instruments. A schematic diagram illustrating this resolution effect is shown in Fig. 1. SCIAMACHY measurements show considerably more spatial detail and yield higher NO_2 columns over pollution hotspots than GOME measurements. Therefore, the inherent spatial heterogeneity of the NO_x fields must be considered when investigating the temporal evolution of vertical tropospheric columns (VCD_{trop}) NO_2 over small, localised areas.

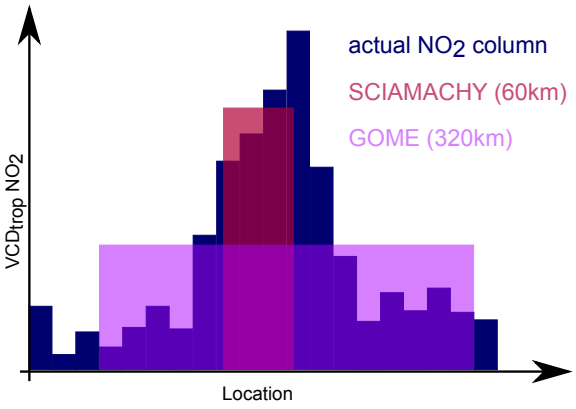

Fig. 1. Schematic view of the effect of the instrument's ground pixel size on the measured VCD_{trop} NO_2.

There have been several studies of the temporal evolution of tropospheric NO_2. The first reports on systematic changes have been published by Richter et al. (2005) and Irie et al. (2005). Konovalov et al. (2006) mathematically convoluted SCIAMACHY measurements, gridded to $1° \times 1°$, to calculate correction factors by which GOME measurements were multiplied, yielding a consistent combined GOME/SCIAMACHY dataset. The study from van der A et al. (2008) fitted a non-linear trend function to ten years of GOME and SCIAMACHY data from megacity regions, modelling the seasonal variation by using one sinus component; they downgraded the SCIAMACHY resolution by convolving over three grid cells (about 300 km). Nine years of SCIAMACHY measurements were analysed by Schneider and van der A (2012), focussing on China and Europe on a country level. Stavrakou et al. (2008) used measurements from GOME and SCIAMACHY to invert anthropogenic NO_x emissions, gridding the measurements to the coarse resolution of the used IMAGES model ($5° \times 5°$). Konovalov et al. (2010) applied non-linear trend analysis to 13 yr of summer measurements from GOME and SCIAMACHY over European urban centres, where SCIAMACHY measurements were convoluted to the spatial resolution of GOME. Hayn et al. (2009) and Zhou et al. (2012) performed extensive studies on the impact of annual and weekly cycles and of meteorology on observed NO_2 columns over Europe, using generalized

[1]To ease notation, we will use the name "GOME-2" as shorthand for the GOME-2 instrument on board Metop-A, as the successor satellites Metop-B and Metop-C had not been launched before the end of our study period.

additive regression models. Several further studies have been published, focussing on certain regions of the world like China (He et al., 2007; Zhang et al., 2007, 2009a), India (Ghude et al., 2008), the megacity Moscow (Sitnov, 2010), coal power stations in the United States (Kim et al., 2006), and international shipping lines (Richter et al., 2004; Franke et al., 2009). Recent studies have been focussing on the impact of NO_x emission reductions due to the global economic crisis and air quality legislation in the United States (Russell et al., 2012), Europe (Castellanos and Boersma, 2012), Greece (Vrekoussis et al., 2013), China (Lin and McElroy, 2011), and for shipping emissions (de Ruyter de Wildt et al., 2012).

In the present study, we provide an update on the global NO_2 trends reported in Richter et al. (2005), propose three alternative methods of handling the issue of different spatial resolution between GOME and SCIAMACHY measurements, and report on NO_2 trends for a number of megacities and large urban agglomerations. The manuscript is structured as follows: in Sect. 2, we describe the dataset of VCD_{trop} NO_2 which we used for this study. A general overview of the changes in tropospheric NO_2 which can be deducted from GOME and SCIAMACHY measurements alone is given in Sect. 3. In Sect. 4 we introduce a physical correction method, which super-imposes the spatial patterns of SCIAMACHY measurements on GOME data to create a consistent high resolution dataset. An alternative, empirical way of deriving trend estimates from the combined dataset by explicitly accounting for the instrumental differences is presented in Sect. 5. This trend model is finally expanded to include measurements from all four available instruments, as described in Sect. 6.

2 Measurements of tropospheric NO_2

The GOME instrument on board the European Research Satellite 2 (ERS-2) was a nadir viewing spectrometer measuring three pixels per forward scan and one back scan. For a 960 km swath width this was the measurement mode for 90 % of the operation; the spatial resolution was 320 km and 40 km in across and along track directions, respectively. 10 % of the time the instrument had a swath width of 240 km and ground scenes of $80 \times 40\,km^2$. The satellite was in a near polar orbit, crossing the equator at 10:30 LT. Global coverage was obtained every three days at the equator (Burrows et al., 1999).

The SCIAMACHY instrument on board the ENVISAT satellite also measured with a swath width of 960 km. While the along track extents of the swath were 30 km, the typical integration time of 0.25 s lead to across-track extents of 60 km for the forward pixels, which we used in this study. ENVISAT circles the Earth on a near polar orbit, crossing the equator at 10:00 LT. SCIAMACHY attained global coverage every six days (Burrows et al., 1995; Bovensmann et al., 1999; Gottwald and Bovensmann, 2011, pp. 22, 56–58).

The Ozone Monitoring Instrument on board the Aura satellite is a wide-field-imaging grating spectrometer, crossing the equator at 13:45 LT ascending mode. Its horizontal resolution is $13 \times 24\,km^2$ at the nadir point, but gets considerably larger with higher viewing angles. The GOME-2 instrument on board the Metop-A satellite covers the Earth's surface with a horizontal resolution of $80 \times 40\,km^2$ with nearly global coverage every day, and an equator crossing at 09:30 LT.

All four instruments measure spectra of extraterrestrial solar irradiance and the upwelling earthshine radiance at the top of the atmosphere. For the GOME, SCIAMACHY, and GOME-2 instruments, these spectra are subsequently analysed using differential optical absorption spectroscopy (Platt and Stutz, 2008) in the 425–450 nm wavelength window (Richter and Burrows, 2002). Absorption cross sections for O_3 (Bogumil et al., 2003), NO_2 (Bogumil et al., 2003), O_4 (Greenblatt et al., 1990), and H_2O (Rothman et al., 1992) are included in the fitting process, as well as the infilling of Fraunhofer lines and molecular absorption known as the Ring Effect (Vountas et al., 1998), an under-sampling correction (Chance, 1998), and for GOME and SCIAMACHY, a calibration function accounting for the polarisation dependency of the instrument's spectral response (Richter and Burrows, 2002). For the determination of the tropospheric NO_2 column amount from the measurements of the OMI instrument, we use the slant columns from NASA's OMI/Aura Nitrogen Dioxide (NO_2) Total & Tropospheric Column1-orbit L2 Swath 13×24 km (Version 3) dataset. The differences between the four instruments are summarised in Table 1.

The stratospheric correction has been carried out using the algorithm detailed by Hilboll et al. (2013a). The Oslo CTM2 used in that study has been replaced with the Bremen 3d CTM (B3dCTM), because the Oslo CTM2 data were only available from 1998–2007. A description of the B3dCTM is given in the Supplement.

Tropospheric air mass factors (AMFs) have been calculated with the radiative transfer model SCIATRAN (Rozanov et al., 2005). The vertical distribution of tropospheric NO_2 has been taken from a climatology of NO_2 mixing ratios from the MOZART2 model (Horowitz et al., 2003), and surface spectral reflectance from GOME measurements (Koelemeijer et al., 2003). Both aspects are explained in detail in Nüß (2005). The AMFs have then been spatially interpolated to a 0.125° grid. Measurements with a cloud coverage exceeding 20 % have been filtered out using the FRESCO+ algorithm (version 6; Wang et al., 2008). Additionally, we applied an intensity filter to discard scenes with very large surface reflectivity. This is necessary as the used albedo or surface spectral reflectance climatology (Koelemeijer et al., 2003) does not account for short-term changes in reflectivity for example from snow; in addition, the FRESCO+ cloud fractions have large uncertainties over bright surfaces.

Table 1. Characteristics of the four satellite platforms used in this study.

Instrument	Equator crossing	Global coverage	Availability period	Pixel size at nadir (km^2)
GOME	10:30 LT	3 days	Oct 1995–Jul 2003	40×320
SCIAMACHY	10:00 LT	6 days	Aug 2002–Apr 2012	30×60
OMI	13:45 LT	1 day	Oct 2004–	13×24
GOME-2	09:30 LT	$\sim$ 1 day	Jan 2007–	40×80

3 Changes in tropospheric NO_2 as observed by GOME and SCIAMACHY

When concatenating annual mean VCD_{trop} NO_2 from GOME (1996–2002) and SCIAMACHY (2003–2011) measurements into one 16 yr time series, many areas of the world show persistent changes. Figure 2 shows this for seven selected regions[2]; the time series are all normalized to the 1996 value to make relative changes comparable. This figure extends the approach used to determine Fig. 1 in Richter et al. (2005), but uses a slightly updated data analysis (e.g. FRESCO+ v6 cloud screening for both instruments, a more recent version of the stratospheric correction model, and a higher spatial resolution of the gridding). All the selected spatial regions show persistent trends, which are downward in the case of Western industrialised countries/regions (United States, Europe, and Japan), and upwards for countries/regions with developing economies like China, India, and in the Middle East. East-central China, for example, has seen a triplication of tropospheric NO_2 columns over the whole time period, while NO_2 values over the central East Coast of the United States have receded by more than 40 %. These changes are explained by two behaviours, which have opposite impacts: continuing success in the reduction of NO_x emissions, in particular from cars and power plants, and increasing emissions from intensified use of the combustion of fossil fuels for energy. In rapidly developing regions such as China, any reductions in specific emissions are overwhelmed by the absolute increase of energy use.

It is important to note, however, that even though the selected areas are all quite large, some of them appear to show small discontinuities in 2003 where the two time series are connected.

The regional trends in satellite observed NO_2 columns are compared to EDGAR NO_x emission data (version 4.2, European Commission, JRC and PBL, 2011) integrated over the same regions (Fig. 3). Initial comparison shows that the sign of direction of changes is the same for all regions in EDGAR and satellite observations. While generally the trend observed in the measured NO_2 columns is more pronounced than in the EDGAR emission inventory, this is not the case for the Middle East and north-central India, which show smaller trends in the data than in the inventory. For east-central China, it is interesting to note that until 2002, the inventory does not significantly increase. Only from 2003 onward, it shows a strong positive trend. This is in contrast to the satellite observations, which show increasing NO_2 values over east-central China from the start of the observation period in 1996 onwards. At the same time, the temporal variability of the NO_x emissions is considerably lower than that of the observed NO_2 columns. This could either be the result of measurement uncertainties, mostly related to year-to-year changes in spatial and temporal sampling of the observations, or indicate inappropriate or inadequate assumptions in the bottom-up inventory. One possible issue in the direct comparison of emission inventories and satellite measurements might be found in the way emission inventories are compiled. Often, country-level emission estimates are spatially redistributed based on activity data. In regions where only limited activity data are available, this might lead to inaccuracies in the spatial distribution of the emissions. On the other hand, changes in NO_2 columns and NO_x emissions are not necessarily related to each other in a linear way, particularly if changes are large (Stavrakou et al., 2008; Lamsal et al., 2011; Konovalov et al., 2010). One also needs to keep in mind that the inter-annual variability of observed NO_2 columns stems to a large part from meteorological variability (Voulgarakis et al., 2010; Hayn et al., 2009). In spite of the qualitative agreement between emission inventory and satellite observations, the unusual behaviour of bottom-up emissions in China before 2003 and the discrepancy between the onset of the consequences of the development in China and India apparent in the measurements but not the inventory need further investigation to identify unambiguously their origin.

In many regions, NO_2 pollution remains a local problem, as is apparent from plotting histograms of VCD_{trop}. Figure 4 shows the temporal evolution of the histograms for some selected regions for the SCIAMACHY time series (2003–2011). For all regions with the exception of east-central China, a large part of the area is characterized by low and moderate NO_2 levels, and only relatively small areas are affected by intense pollution. Comparing the distributions in different years, it is clearly visible that economic growth and

[2]The north-central Indian industrial region extending between the cities of New Delhi and Lahore lies partly within an area for which GOME measurements are not available because of platform calibration made by ERS-2 in this region. Therefore, this region had to be selected quite small.

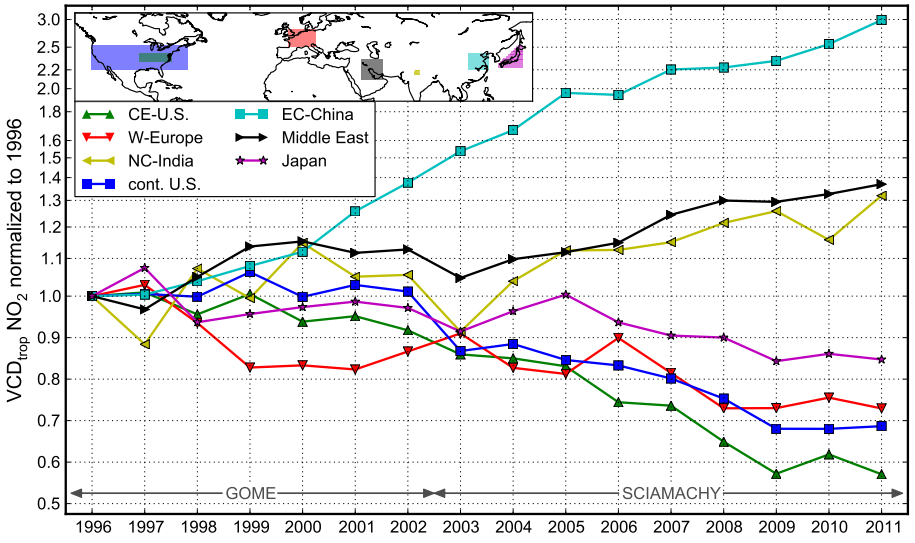

Fig. 2. Mean annual VCD_{trop} NO_2 normalized to 1996 for the regions central East Coast US, Western Europe, US, east-central China, Japan, Middle East, and north-central India. Values for 1996–2002 are from GOME; values from 2003–2011 are from SCIAMACHY measurements. The first five regions are defined as in Richter et al. (2005). The y-axis has been modified to make relative changes above and below 1 more comparable (values larger than 1 have been scaled to $y \mapsto 2 - \frac{1}{y}$).

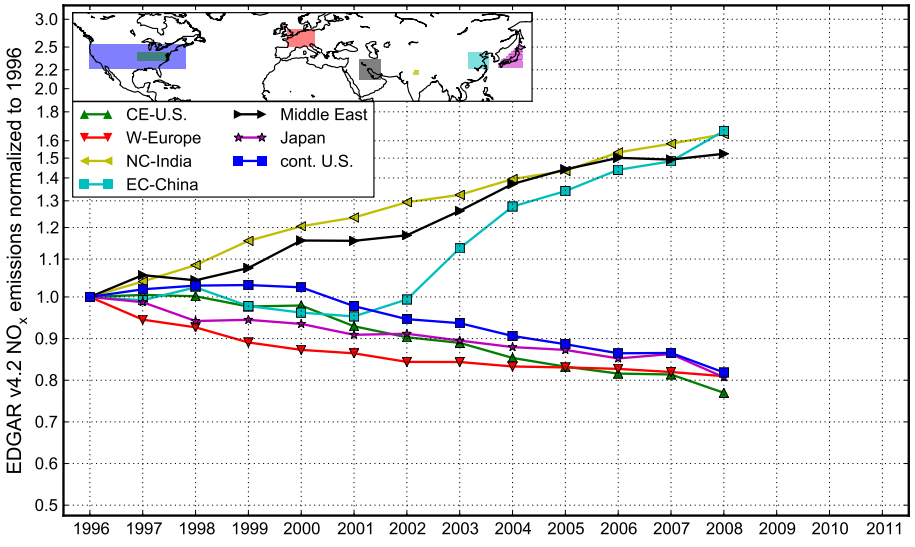

Fig. 3. NO_x emissions from the EDGAR v4.2 database, normalized to 1996, for the regions central East Coast US, Western Europe, US, east-central China, Japan, Middle East, and north-central India. The y-axis has been modified to make relative changes above and below 1 more comparable (values larger than 1 have been scaled to $y \mapsto 2 - \frac{1}{y}$). Since the published version 4.2 of the EDGAR database contains erroneous emission data for the year 2008 in Iran, this plot uses an updated, so far unpublished, version (G. Maenhout, personal communication, 2012) for the Middle East region.

emission control measures and the resulting increases and decreases in the observed VCD_{trop} impact not only pollution hotspots, but regions as a whole. Over east-central China, for example, the fraction of areas with exceptionally high NO_2 levels has been significantly increasing during the observing period, leading to a shrinking area which can be considered as being polluted at lower levels. Over the same period, the central Eastern US has seen systematic increases in the fraction of low or moderately polluted areas.

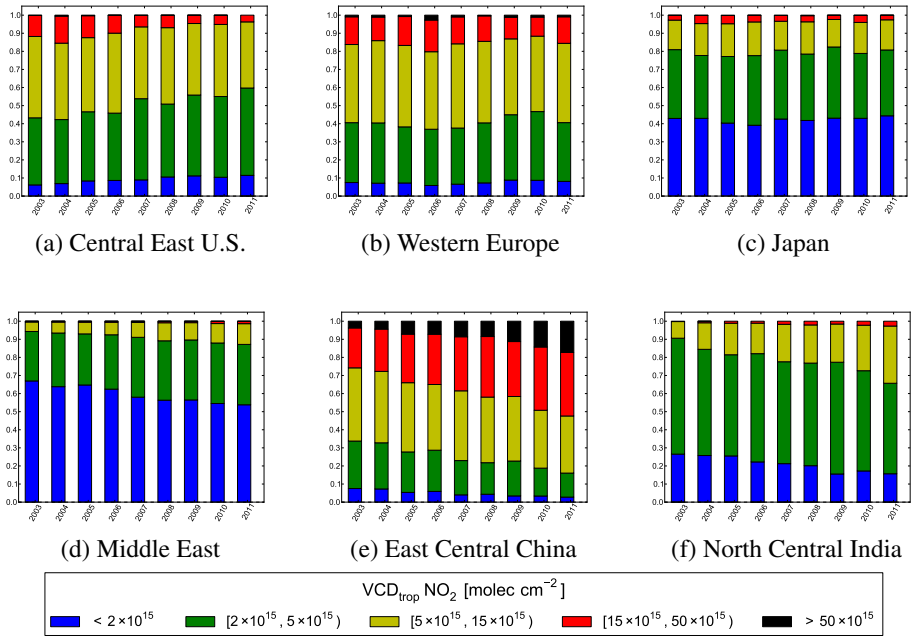

Fig. 4. Histogram of VCD_{trop} NO_2 from SCIAMACHY over the regions from Fig. 2 for the years 2003–2011. The plot shows the relative counts of background (blue), moderately polluted (green), polluted (yellow), very polluted (red), and extremely polluted (black) $1° \times 1°$ grid cells per region.

4 Explicitly correcting for the difference in ground pixel size between GOME and SCIAMACHY measurements

In order to create a consistent dataset of NO_2 measurements at high spatial resolution, the difference in the area of the ground scene or spatial footprint of the measurements made by the GOME and SCIAMACHY instruments needs to be accounted for. Previous studies have either degraded the resolution of both datasets to a level where differences can be ignored, or applied an ad hoc deconvolution of gridded GOME data (Konovalov et al., 2006). In this study, high spatial resolution SCIAMACHY spectra have been averaged to cover a similar area as individual GOME observations. Comparison of the high and low resolution analysis then provides an empirical correction function or factor, which can be applied to GOME data. For this, we make the assumption that the difference between GOME and SCIAMACHY measurements of VCD_{trop} only depends on the size difference between the two instruments' ground pixels and on season. This allows us to simulate measurements with GOME's spatial resolution using SCIAMACHY measurements by averaging over five adjacent spectra. A similar approach has previously been introduced by Beirle et al. (2004), who applied this methodology to GOME measurements, using the instrument's narrow swath mode.

4.1 Method

Based on these assumptions, we calculate a monthly climatology of correction factors which describe the difference between the two instruments. To approximately match the GOME pixel size of $320 \times 40\,km^2$, we average the measured spectra from five adjacent SCIAMACHY forward scan ground pixels with an effective size of $300 \times 30\,km^2$, which yields three enlarged ground pixels per forward scan. On these enlarged ground pixels, we then perform a regular DOAS fitting procedure with the same settings as used for the regular retrieval to obtain a dataset of SCD_{tot} from reduced resolution. This dataset we further process in a fashion identical to that used for the original SCD_{tot}, which in the end yields a set of VCD_{trop} NO_2 from SCIAMACHY measurements with reduced resolution.

This approach has the advantage of providing an appropriate end-to-end simulation of the effects of spatial resolution change, including the impact of change in cloud statistics on the fit, the specific orientation of the satellite ground pixels, and the details of the a priori databases used. The only issue which could not be fully simulated is the change in FRESCO+ cloud fraction, which was approximated by using the average of the individual cloud fraction values. As these values are only used for screening of cloudy scenes, the impact of this approximation is assumed to be small.

Both datasets (regular and reduced resolution) of VCD_{trop} are then gridded globally to a $\frac{1}{16}° \times \frac{1}{16}°$ grid and compiled into monthly averages for the months t' from January

2003 to December 2011. From these two monthly datasets, we calculate the climatological means $\mathrm{VCD}^{\mathrm{SCIA}}(t, \vartheta, \varphi)$ and $\mathrm{VCD}^{\mathrm{SCIA}}_{\mathrm{red.res.}}(t, \vartheta, \varphi)$, where $t = 1, \ldots, 12$ are the months from January to December, and ϑ and φ are latitudes and longitudes, respectively. From these monthly climatologies, we derive the climatological correction factors (ratios),

$$\Gamma(t, \vartheta, \varphi) = \frac{\mathrm{VCD}^{\mathrm{SCIA}}(t, \vartheta, \varphi)}{\mathrm{VCD}^{\mathrm{SCIA}}_{\mathrm{red.res.}}(t, \vartheta, \varphi)}. \quad (1)$$

The gridded monthly averages of the GOME measurements are subsequently multiplied with the appropriate ratio grid of correction factors to yield the resolution-corrected GOME $\mathrm{VCD}_{\mathrm{trop}}$ NO_2:

$$\mathrm{VCD}^{\mathrm{GOME}}_{\mathrm{corr.}}(t', \vartheta, \varphi) = \Gamma(t(t'), \vartheta, \varphi) \times \mathrm{VCD}^{\mathrm{GOME}}(t', \vartheta, \varphi). \quad (2)$$

It should be noted that, in principle, this correction for ground pixel size could also be applied to measurements from other satellite instruments. This would however only be of limited use in the analysis of long-term time series: firstly, correcting GOME measurements to have the spatial resolution of the GOME-2 instrument would leave a gap of 3.5 yr (from 2003–2006) in the combined time series. Furthermore, with larger temporal gaps between the individual instruments' measurement periods, the influence of temporal changes to the spatial distribution of tropospheric NO_2 would increase the uncertainties of the resulting resolution-corrected NO_2 columns. Moreover, in the case of OMI, the influence of the difference in local measurement time would blend with the effects of the different spatial resolutions.

4.2 Spatial variation of Γ

The resolution correction factor Γ is a measure for the spatial heterogeneity of the observed NO_2 signal. Values of Γ larger than 1 indicate that typically observed NO_2 columns at a location are higher than in the surrounding area[3]. Figure 5 shows the global distribution of the annual mean, $\bar{\Gamma}(\vartheta, \varphi) = \frac{1}{12}\sum_t \Gamma(t, \vartheta, \varphi)$, of the resolution correction factor climatology. Over the open oceans, the signal of Γ is noisy. This is related to the large relative errors of the very low measured $\mathrm{VCD}_{\mathrm{trop}}$ NO_2 over the oceans, which are close to or below the instruments' detection limits. Over land, however, and especially in regions with high spatial gradients in NO_2 emissions, such as the United States and Europe, the maxima in the gridded values for Γ clearly coincide with urban agglomerations or conurbations (see Fig. 6). While noisy, a line of enhanced values of Γ can be distinguished over the Atlantic Ocean, running from the tip of north-western France to north-western Spain. This coincides with a major shipping line, whose NO_2 emissions have previously been discovered in satellite imagery (Richter et al., 2004; Franke et al., 2009; de Ruyter de Wildt et al., 2012). Especially in the Western US, where NO_x emissions tend to be very sparsely distributed, local maxima in Γ can be attributed to individual sources like coal power stations. As it is to be expected, local minima of the correction factor are visible longitudinally adjacent to these maxima (see Fig. 6), which is in good agreement with the findings by Beirle et al. (2004).

[3]While this is true both along-track and across-track, the local variability in across-track direction has stronger impact on Γ.

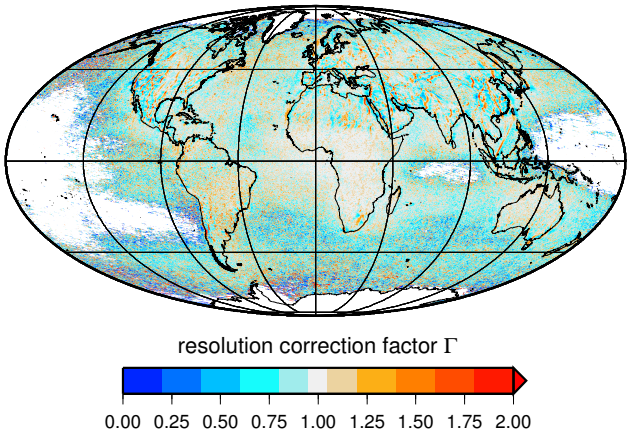

Fig. 5. Annual mean $\bar{\Gamma}$ of the resolution correction factor climatology (2003–2011). Pixels with a mean $\mathrm{VCD}^{\mathrm{SCIA}}_{\mathrm{red.res.}}$ lower than the instrument precision (estimated to be 10^{14} molec cm^{-2}) have been excluded from the plot.

4.3 Validation of the resolution correction

In many cases, the resolution correction works extremely well. This can be evaluated using data from the period of overlapping measurements of the GOME and SCIAMACHY instruments (August 2002–June 2003). To reduce the impact of temporal sampling, only data points for which both instruments have measurements on the same day are included in the validation. For Europe, Fig. 7 compares original GOME and SCIAMACHY measurements to spatially down-sampled SCIAMACHY and resolution-corrected GOME measurements. The spatial distribution of GOME measurements is well approximated by the down-sampled SCIAMACHY measurements. Furthermore, the greater spatial detail inherent to the gridded SCIAMACHY measurements is obviously well transferred to the resolution-corrected GOME measurements.

A more detailed comparison over pollution hotspots is provided in Fig. 8, which shows the monthly mean values of $\mathrm{VCD}_{\mathrm{trop}}$ NO_2 for the four cities Mumbai, Seoul, Mexico City, and Rome[4]. While in the direct comparison there are differences of up to a factor of two, most of the corrected GOME data agree with SCIAMACHY data within

[4]Depending on the extent of the urban sprawl, the individual city regions have been defined as rectangles with edge lengths between 0.5° and 1.0°.

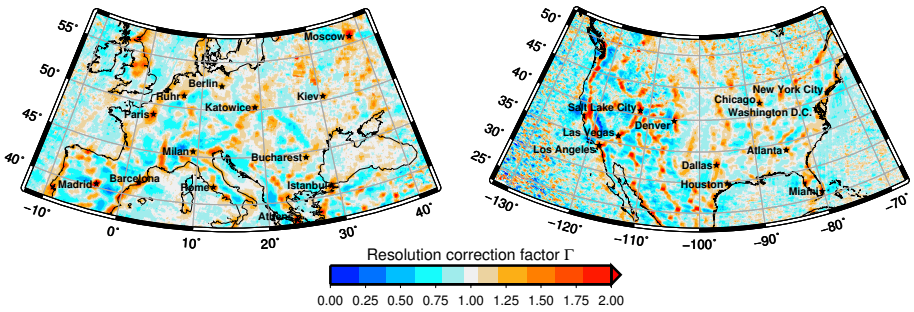

Fig. 6. Annual mean $\bar{\Gamma}$ of the resolution correction factor over the United States (right) and Europe (left).

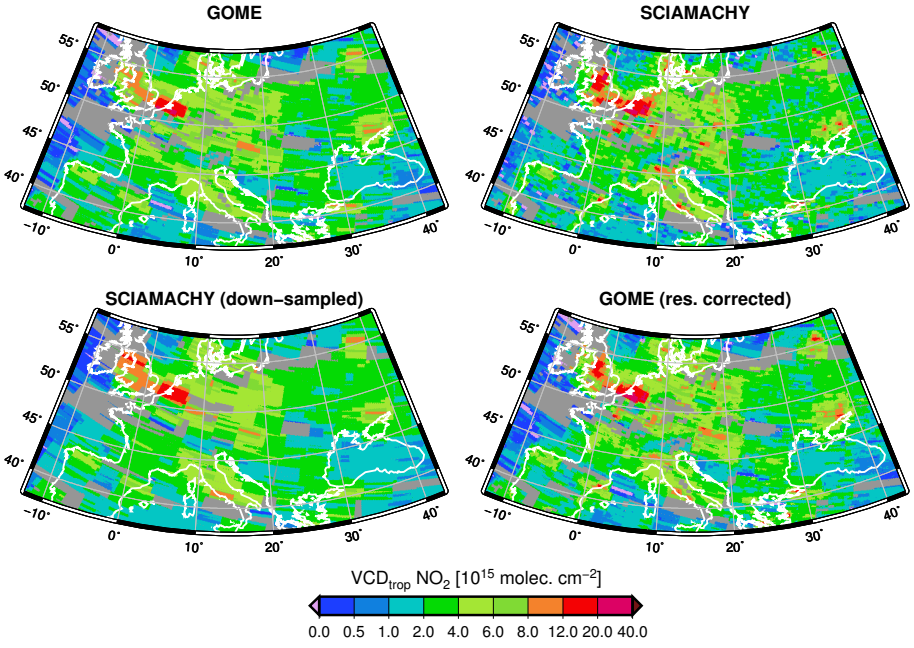

Fig. 7. Tropospheric NO_2 columns from GOME (top left), SCIAMACHY (top right), down-sampled SCIAMACHY (bottom left), and resolution-corrected GOME (bottom right) measurements for May 2003, gridded to $\frac{1}{16}° \times \frac{1}{16}°$. The effect of spatial smoothing can be seen in the original GOME and the down-sampled SCIAMACHY measurements for all point-like sources like cities, as the signal becomes smeared out.

10 %, independent of season. Quite often, however, the correction method actually overshoots, which leads to unreasonably high VCD_{trop} NO_2 for the corrected GOME measurements, especially over urban areas. As an example, the four cities Houston, Baghdad, Cairo, and Karachi are shown in Fig. 9. When performed over larger areas, a small overcorrection is also observable in some months (see Fig. 10).

4.4 Discussion

The apparent over-correction in some situations is initially at least unexpected, as from the approximations made, one would expect the correction to underestimate the resolution effect, because the SCIAMACHY pixels with reduced resolution still only cover about 70 % of the ground area of a GOME measurement. There are several possible reasons for the observed differences: a problem with the approach used for resolution correction, a bias in one or both of the datasets, or real NO_2 differences, for example from the different overpass times of the two satellites, which could lead to systematically different NO_2 columns.

For most investigated areas, down-sampled SCIAMACHY measurements agree extremely well with original GOME measurements (see Figs. 8–10), showing that the derived resolution correction factor Γ should in principle well capture the differences between the two instruments which are due to their respective spatial resolutions.

As a next check, we investigated whether DOAS analysis of the spatially averaged SCIAMACHY spectra actually yields the same mean SCD_{tot} NO_2 as obtained from the regular measurements. The results for 4 exemplary orbits from the year 2011 are shown in Table 2. We chose the open

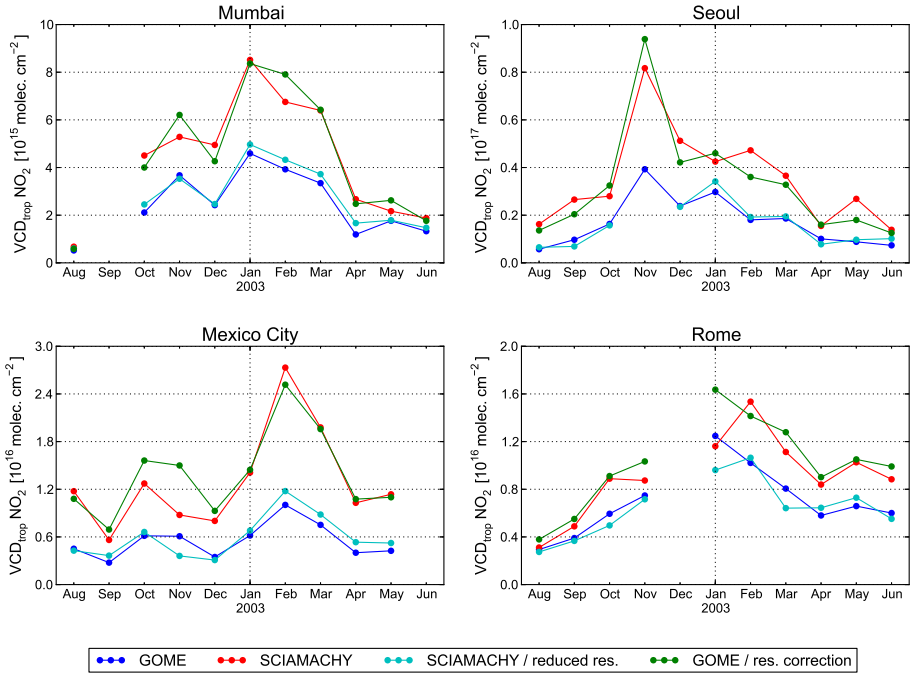

Fig. 8. Monthly averages of VCD_{trop} NO_2 over four exemplary areas showing very good agreement between corrected GOME and original SCIAMACHY measurements, for the time period August 2002–June 2003. Only those days for which both GOME and SCIAMACHY measurements for a city are available are taken into account.

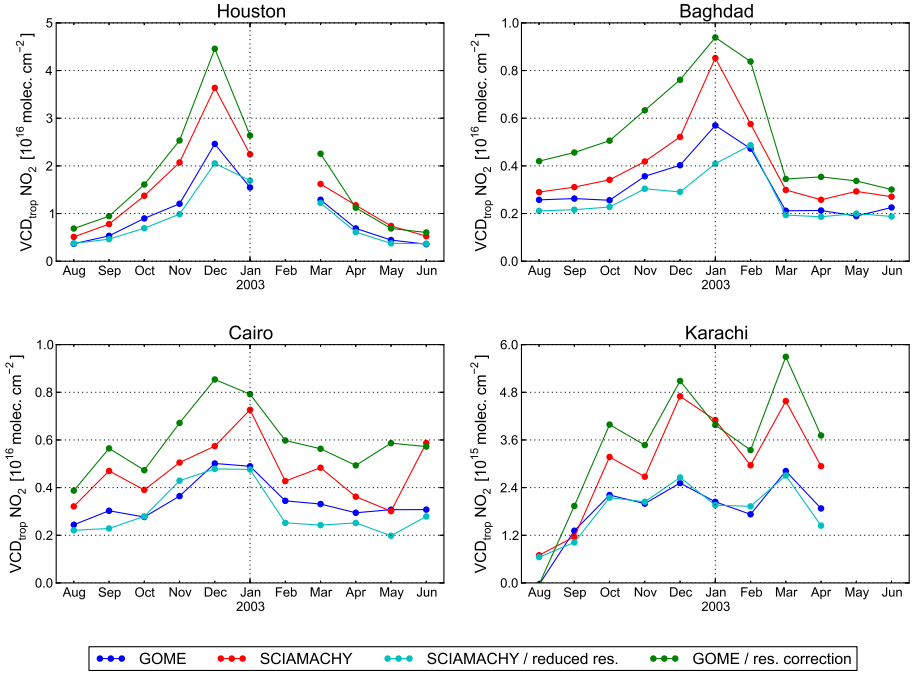

Fig. 9. Monthly averages of VCD_{trop} NO_2 over four exemplary areas showing a significant over-correction, for the time period August 2002–June 2003. Only those days for which both GOME and SCIAMACHY measurements for a city are available are taken into account.

Pacific Ocean for this first test because in this pristine region we expect spatially homogeneous NO_2 measurements. As the measured slant columns agree almost perfectly in most cases, we conclude that for homogeneous scenes, the spatial averaging of the measured spectra does not influence the magnitude of the retrieved VCD_{trop}.

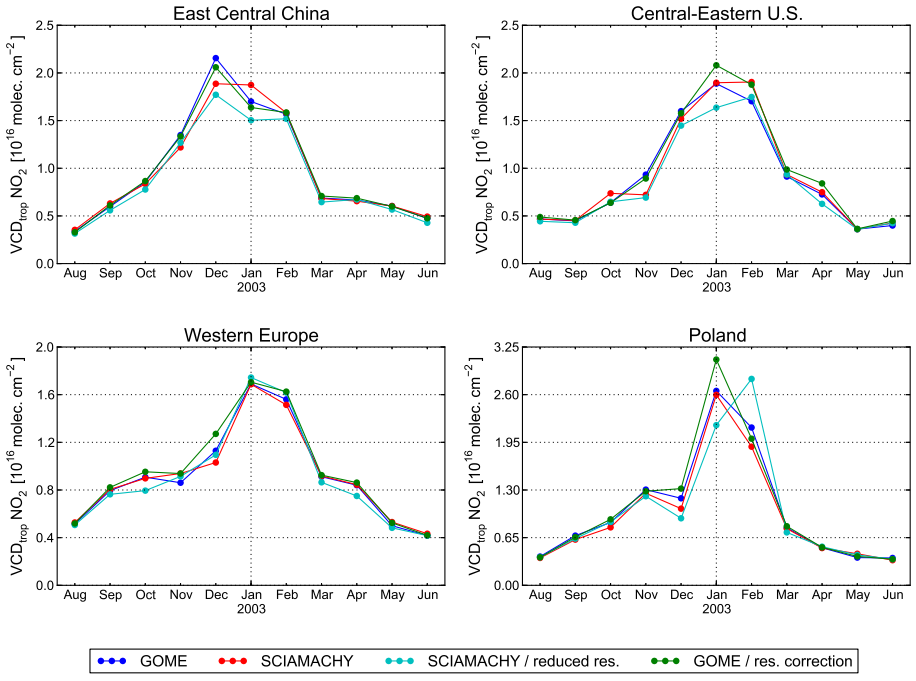

Fig. 10. Monthly averages of VCD_{trop} NO_2 over four country- to continental-scale areas, for the time period August 2002–June 2003. The regions are the same as used in Richter et al. (2005). Only those days for which both GOME and SCIAMACHY measurements for a city are available are taken into account.

Table 2. Relative difference of original SCIAMACHY measurements $SCD^{SCIA}(\vartheta, \varphi)$ and reduced-resolution SCIAMACHY measurements $SCD^{SCIA}_{red.res.}(\vartheta, \varphi)$ for four exemplary orbits from the year 2011.

Relative difference $\frac{SCD^{SCIA}(\vartheta,\varphi)}{SCD^{SCIA}_{red.res.}(\vartheta,\varphi)} - 1$ (%)				
Orbit number	46 222	47 514	48 821	50 143
Latitude range	1 Jan 2011	1 Apr 2011	1 Jul 2011	1 Oct 2011
90° S–80° S	−0.15	+0.00	n/a	+0.75
80° S–70° S	+4.1	−16.0	n/a	+2.6
70° S–60° S	+1.0	+2.7	−6.1	+0.68
60° S–50° S	+0.90	+0.87	+2.3	+0.44
50° S–40° S	+0.75	+2.2	+1.7	+0.49
40° S–30° S	+0.12	+0.59	+0.92	+2.3
30° S–20° S	−0.32	+0.23	+1.2	+0.59
20° S–10° S	−0.34	+0.29	−0.54	+0.51
10° S–0°	+0.28	−0.29	−0.051	+0.35
0°–10° N	+0.75	+1.1	+0.054	+0.062
10° N–20° N	+0.47	+0.056	+0.063	+0.62
20° N–30° N	+0.12	+0.086	−0.11	+0.36
30° N–40° N	+0.51	+0.11	+0.080	+0.62
40° N–50° N	+0.61	−0.014	+0.38	+0.25
50° N–60° N	+0.29	+0.33	+0.66	+0.64
60° N–70° N	−16.0	+1.2	+0.90	+0.22
70° N–80° N	+3.8	−1.0	+2.3	−6.3
80° N–90° N	n/a	−2.4	+0.83	−17.0

When repeating the same test for regions affected by the over-correction, e.g. the relatively isolated pollution hotspot formed by the city of Cairo in northern Egypt, we find that even when considering an area as large as $4° \times 5°$, original SCIAMACHY measurements give an up to 10 % higher average than those with down-sampled spatial resolution. This suggests that for heterogeneous ground scenes, an averaging of the measured spectra is not always equivalent to an averaging of the actual NO_2 columns, and hints towards non-linearities in the approach. These effects might be enhanced by the application of tropospheric air mass factors, potentially partly caused by the low spatial resolution of the AMFs.

As this effect is most often observed for cities in desert-like areas, one could also speculate that the spectral signature of bare soil, which was shown to influence NO_2 DOAS retrievals by Richter et al. (2011), is differently captured by the GOME and SCIAMACHY instruments and thus leads to the observed over-correction.

Since the resolution correction factors are calculated from the NO_2 columns measured by SCIAMACHY during the years 2003–2011, they represent the average spatial distribution of this time period. For cities with large temporal NO_2 changes, this can potentially lead to inaccuracies when the average spatial structure of 2003–2011 is superimposed on measurements from 2002/2003 and before. Rapid changes, such as construction of new power plants, growth of cities, or implementation of NO_x reduction technologies may change the spatial pattern of NO_2 on the scales resolved

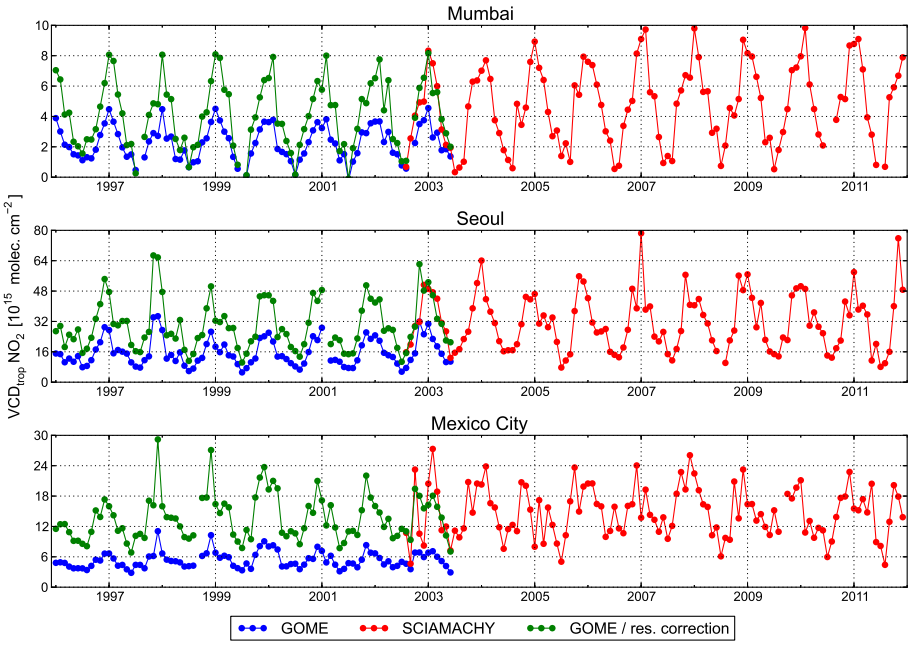

Fig. 11. Time series of original GOME (blue), resolution-corrected GOME (green), and SCIAMACHY (red) measurements of tropospheric NO_2 for the three selected megacities Mumbai, Seoul, and Mexico City.

by SCIAMACHY, leading to biases in the GOME resolution correction. However, analysis of annual (instead of climatologically averaged) resolution correction factors did not yield firm evidence for such systematic effects, at least not within the uncertainty of the values.

The potential influence of the difference in measurement times could in principle be investigated using GOME measurements from the instrument's narrow swath mode. In practice, the small number of such measurements and the different temporal sampling compared to normal instrument operation make an interpretation of the results very challenging.

For most investigated cities, the resolution correction factor is a valuable tool to combine NO_2 measurements from GOME and SCIAMACHY consistently, as it is able to capture the impact of the different instrumental resolutions very well. After applying it to GOME measurements, combined time series of tropospheric NO_2 columns do not show instrumental differences anymore in many cases (Fig. 11), allowing for the first time the evaluation of long-term NO_2 trends over local hotspots.

5 Fitting a trend model accounting for the difference between GOME and SCIAMACHY measurements

An alternative approach to evaluate the combined time series for temporal changes is to use a trend model which includes a parameter allowing for adjustments between the two datasets. Such an analysis is not based on modelling the physical process of spatial averaging but has the advantage of accounting also for other differences between the datasets and of providing a more rigorous error assessment. In order to account for the systematic difference between GOME and SCIAMACHY measurements, we follow the approach proposed by Mieruch et al. (2008) for the analysis of global water vapour trends. The method is based on the work of Weatherhead et al. (1998) and Tiao et al. (1990), and explicitly accounts for the instrumental difference with a level shift parameter in the fitting procedure.

5.1 Method

The trend model explicitly accounts for (a) a level shift between the two instruments and (b) for a change in the amplitude of the seasonal variation. In brief, the time series of monthly averages of NO_2 measurements $Y(t)$ is described by the equation

$$Y(t) = \mu + \omega t + \delta U(t) + S(t) + N(t), \tag{3}$$

where μ is the VCD_{trop} measurement at time $t = 0$, ω is the monthly trend component, and t is the time in months since January 1996. δ is the level shift between GOME and SCIAMACHY measurements occurring at time $t = T_0$ (which we set to January 2003), and $U(t)$ is the step function

$$U(t) = \begin{cases} 0, & t < T_0 \\ 1, & t \geq T_0. \end{cases} \tag{4}$$

The seasonal component $S(t)$ has the same shape (represented by harmonic functions) and varying amplitude for the

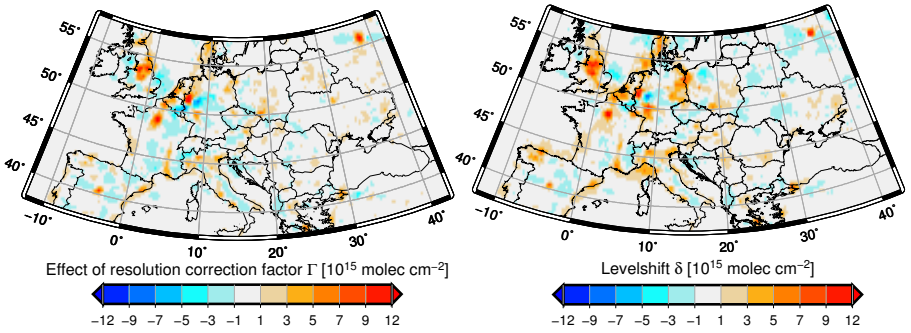

(a) Effect of resolution correction factor Γ: $VCD^{GOME}_{corr.} - VCD^{GOME}$ for the year 2002

(b) Levelshift offset δ

Fig. 12. Comparison of the effects of resolution correction factor Γ (applied to average GOME measurements from 2002) and level shift offset δ.

two instruments, and is modelled by

$$S(t) = (1 + (\gamma - 1)\,U(t)) \sum_{j=1}^{4} \left(\beta_{1,j} \sin\left(\frac{2\pi jt}{12}\right) + \beta_{2,j} \cos\left(\frac{2\pi jt}{12}\right)\right), \quad (5)$$

where the term $(\gamma - 1)U(t)$ describes the amplitude change of the seasonality component at the change between the instruments. $N(t)$, finally, is the noise component, i.e. the part of the time series which cannot be explained by the underlying model.

The trend estimator $\hat{\omega}$ is calculated in a two-step procedure: first, the noise components $N(t)$ are derived by solving Eq. (3) for those estimators, $\hat{\mu}$, $\hat{\omega}$, $\hat{\delta}$, and $\hat{\gamma}$, which lead to minimal $N(t)$. After subtracting the seasonal component $S(t)$, which usually has negligible effect on the estimation of the other trend parameters (Weatherhead et al., 1998), the autocorrelations are accounted for using a linear matrix transformation. Finally, linear regression is applied to derive the estimators $\hat{\mu}$, $\hat{\omega}$, $\hat{\delta}$, and $\hat{\gamma}$ (Mieruch et al., 2008).

For the estimation of the trend error, we assume the noise process $N(t)$ to be AR(1), i.e. autoregressive with lag 1. The autocorrelation in the noise is accounted for in the error calculation as detailed in Mieruch et al. (2008). The trend is assumed to be significant if and only if

$$P_{H_0}\left(|\hat{\omega}| > 2\sigma_{\hat{\omega}}\right) = \mathrm{erf}\left(\frac{|\hat{\omega}|}{\sigma_{\hat{\omega}}\sqrt{2}}\right) > 95\,\%, \quad (6)$$

with

$$\mathrm{erf}(x) = \frac{2}{\sqrt{\pi}} \int_0^x e^{-t^2}\,\mathrm{d}t \quad (7)$$

being the Gauss error function.

5.2 Comparison of resolution correction factor Γ and level shift parameter δ

As both the resolution correction factor Γ and the level shift parameter δ are measures for how large the tropospheric NO_2 content at a given point is compared to its surrounding area, the two datasets should show large similarities. Indeed, as shown in Fig. 12, the maps of the respective impacts of Γ and δ are in very good agreement. For example, large urban agglomerations, such as Madrid, Paris, Moscow, and Istanbul, are clearly visible in both datasets. As the two methods are unconnected and only depend on the satellite measurements, we conclude that both techniques are legitimate approaches to overcome the issue of varying pixel sizes when combining measurements from GOME and SCIAMACHY. However, the level shift can also account for other, non-resolution-related differences between the two datasets.

If the resolution correction method described in Sect. 4 worked perfectly well, the application of the level shift trend model (Eq. 3) to resolution-corrected GOME measurements $VCD^{GOME}_{corr.}$ and SCIAMACHY measurements VCD^{SCIA} should yield a level shift δ equivalent to the instrumental bias between GOME and SCIAMACHY measurements, which is assumed to be negligibly small. In practice, the resolution correction only produces valid results when the actual tropospheric NO_2 column is considerably larger than the instrument's detection limit, as pointed out in Sect. 4.2. In Fig. 13, we compare the spatial distribution of the level shift offset δ calculated for the original and the resolution-corrected GOME datasets. As expected, the original data show a characteristic pattern of positive and negative level shifts δ over and adjacent to pollution hotspots, respectively, along the east and south coasts of the Japanese main island Honshu and over South Korea. These patterns dissolve when the level shift model is applied to resolution-corrected GOME measurements. However, the level shift does not totally vanish. While over Japan and the Korean Peninsula δ is reduced significantly and close to zero in the resolution-corrected dataset, the area around Shanghai in eastern China still shows enhanced level shifts of $10–14 \times 10^{15}$ molec cm^{-2}, which is about 40 % lower than in the original dataset. One possible explanation is the temporal changes in the spatial NO_2 patterns, which cannot be accounted for using the

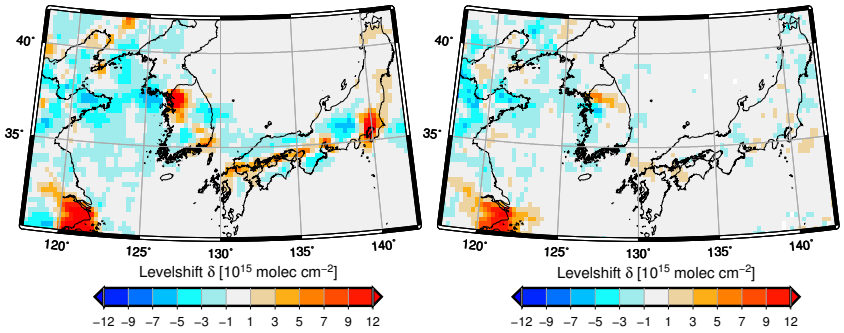

Fig. 13. Comparison of level shift offset δ between the original (left) and resolution-corrected (right) GOME measurements and the SCIAMACHY dataset.

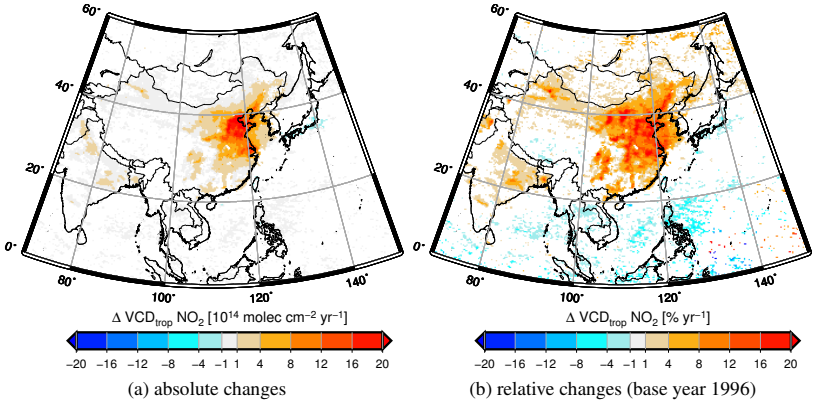

Fig. 14. Annual change in VCD_{trop} NO_2 over China derived from the level shift trend model for the years 1996–2011. The maps show the statistically significant values of the linear trend component ω from the level shift model (Eq. 3) in absolute values **(a)** and relative changes **(b)**.

resolution correction factor (see Sect. 4.4). As it can be seen from Fig. 14, the largest changes in tropospheric NO_2 columns in the Shanghai area do not happen in the city itself, but rather north-west of Shanghai. Most of these changes are due to a steep increase in the years 2002–2005. This results in a decrease of the spatial NO_2 gradient over time, and consequently, the resolution correction factor calculated from the 2003–2011 climatology is too low for the stronger spatial gradients of the 1996–2002 period. As a result, a clearly visible gap between GOME and SCIAMACHY measurements remains in the time series for Shanghai, which results in the large level shift which can be observed.

5.3 Global distribution of tropospheric NO_2 changes

The level shift model has been applied to the combined dataset of GOME (January 1996–December 2002) and SCIAMACHY (January 2003–December 2011) measurements. The results show strong and significant changes in tropospheric NO_2 columns for large areas in North America, Europe, the Middle East, China, Japan, and India (see Fig. 15). While Western countries have experienced strongly decreasing VCD_{trop} NO_2 during the past 16 yrs, developing countries like India, China, and in the Middle East, show strongly increasing NO_2 columns. Over the United States, large decreases can be observed for the Los Angeles metropolitan area and for large parts of the Eastern US. There, the areas with the largest reductions coincide with those areas already shown to be strongly affected by power plant emission reductions (see Kim et al., 2006). In the Middle East, the large increases are limited to large urban agglomerations, like the cities of Damascus, Baghdad, Kuwait City, Tehran, Isfahan, Riyadh, Jeddah, Cairo, Doha, and Dubai. For the regions defined in Fig. 2, the results are summarised in Table 3. All these observations are in good agreement with the general findings presented in Sect. 3, and are backed by Granier et al. (2011), who report according trends in NO_x emissions in all major emission inventories.

The results from the combined GOME/SCIAMACHY dataset can be compared to trends which are derived from GOME or SCIAMACHY measurements alone, as shown in Fig. 16. Obvious differences can be identified for North America, Europe, and China. Over the East Coast of the US, the largest annual decreases in tropospheric NO_2 columns can be observed in the SCIAMACHY time series. In Europe,

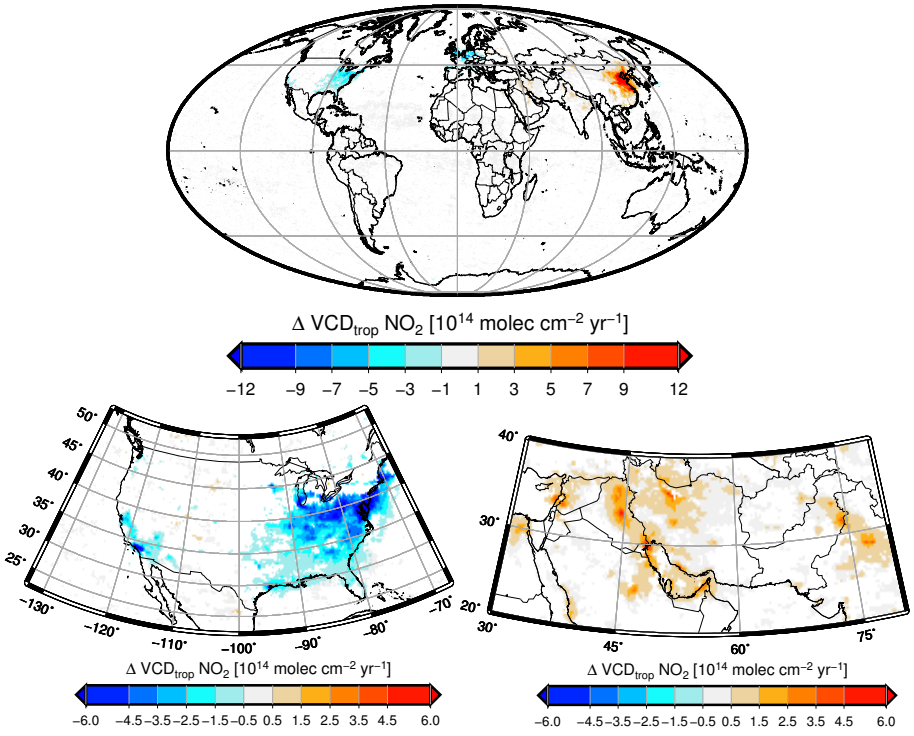

Fig. 15. Slope ω of the linear trend component of the level shift trend model (Eq. 3) applied to monthly averages of GOME and SCIAMACHY measurements from 1996–2011, gridded to 0.25°. Those grid cells where the two-sided p value for a hypothesis test whose null hypothesis is that the slope is zero is larger than 0.05 are excluded from the plot.

Table 3. Annual growth rate ΔVCD$_{trop}$ NO_2 from the level shift model (Eq. 3) and the multi-instrument fit (Eq. 9) for the regions shown in Fig. 2. The relative trends have been computed relative to the 1996 annual mean.

Region	Level shift model (orig. GOME data)		Multi-instrument fit	
	$[10^{14}\,\mathrm{molec\,cm^{-2}\,yr^{-1}}]$	$[\%\,\mathrm{yr^{-1}}]$	$[10^{14}\,\mathrm{molec\,cm^{-2}\,yr^{-1}}]$	$[\%\,\mathrm{yr^{-1}}]$
Continental US	-0.81 ± 0.14	-1.72 ± 0.30	-0.78 ± 0.20	-1.66 ± 0.42
Central Eastern US	-2.94 ± 0.38	-2.96 ± 0.38	-2.65 ± 0.47	-2.69 ± 0.48
Western Europe	-2.94 ± 0.63	-2.61 ± 0.56	-2.63 ± 0.85	-2.35 ± 0.76
Japan	-0.49 ± 0.13	-1.24 ± 0.33	-0.49 ± 0.17	-1.24 ± 0.42
Middle East	$+0.779 \pm 0.082$	$+4.00 \pm 0.42$	$+0.727 \pm 0.093$	$+3.70 \pm 0.47$
East-central China	$+10.1 \pm 1.1$	$+20.5 \pm 2.2$	$+8.7 \pm 1.2$	$+16.3 \pm 2.2$
North-central India	$+1.30 \pm 0.27$	$+4.05 \pm 0.84$	$+1.05 \pm 0.32$	$+3.23 \pm 0.98$

the GOME time series shows considerably larger decreases in VCD$_{trop}$ NO_2 than both the SCIAMACHY and the combined time series. At the Chinese east coast, finally, the area showing large annual increases is considerably larger in the SCIAMACHY period than in the GOME time series. This observation is consistent with the observed increase in the fraction of highly polluted areas in China (see Fig. 4), and is backed by a comparison of absolute to relative changes, as shown in Fig. 14. While in the absolute changes, the well-known area of east-central China shows the largest upward trend, the spatial distribution of the relative changes is more homogeneous, and the largest relative increases are actually seen at the margins of the area with the highest NO_2 columns. Large annual increases of 10 % and more can be observed in extended areas. Apart from the Chinese coastal area, which hosts the bulk of the nation's economic activities and is known for its high levels of air pollution, other regions show large relative trends as well. Especially in Inner Mongolia and Xingjiang, and in the Ningxia, Shaanxi, and Gansu regions of central China, large relative growth rates of tropospheric NO_2 columns can be observed. As these areas still show relatively low VCD$_{trop}$ NO_2, they do not stand out in the absolute annual increases. It should however be noted that especially in these regions of large economic growth, new point sources (e.g. power plants) can be constructed, and

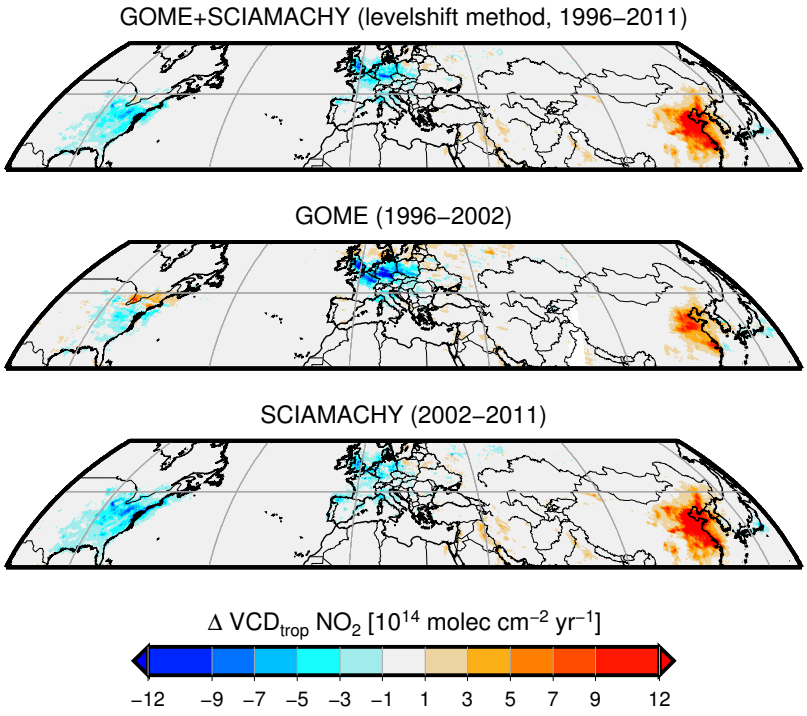

Fig. 16. Slope ω of the level shift model (Eq. 3, top) and of the seasonality model (Eq. 3 without the level shift terms $\delta U(t)$ and $(\gamma-1)U(t)$), applied to monthly averages of GOME (centre) and SCIAMACHY (bottom) measurements alone. All data have been gridded to 0.25° before performing the model fit. In contrast to Fig. 15, statistically insignificant trends have not been masked out.

their new emissions will show up as large non-linear relative growth rates.

Another interesting aspect in Fig. 14 is the large increase of NO_2 over the Yellow Sea between China and Korea. This NO_2 is attributed to transport of air from the polluted regions on land and gives an idea of the impact of transport on the NO_2 fields observed in countries downwind of China. Any increases in emissions from shipping also need to be considered. It is noteworthy to also point out that the effect of transport of air pollution also limits the spatial resolution of the satellite NO_2 maps, in particular in winter.

The differences between the trends in the GOME and SCIAMACHY time periods indicate an overall problem with the assumption of linear trends in NO_x emissions and NO_2 columns. As emissions are controlled by technological, political, and economic factors, rapid, non-linear changes have to be expected. This issue has already been raised by Konovalov et al. (2010), but for most regions, the length of the time series in combination with the uncertainties of the individual values does not yet allow for reliable detection of the non-linear component of the observed changes. However, for individual time series over selected regions (i.e. Los Angeles and Athens), the non-linearity is obvious and has to be taken into account when interpreting the data (Vrekoussis et al., 2013; Russell et al., 2012).

5.4 VCD_{trop} NO_2 over megacities

The level shift trend model facilitates the investigation of the development of individual pollution hotspots' NO_2 abundances. As it does not require the spatial down-sampling applied in previous studies (van der A et al., 2008; Konovalov et al., 2010), accurate estimation of the temporal evolution of NO_2 pollution of localised sources becomes feasible. We summarise the trend estimates for a variety of megacities in Table 4 and in the Supplement. The strongest relative upward trends are visible over the cities of Dhaka in Bangladesh and Baghdad in Iraq, at $+27.2 \pm 3.9\,\%\,yr^{-1}$ and $+20.7 \pm 1.9\,\%\,yr^{-1}$, respectively, which is in agreement with Schneider and van der A (2012). The apparent difference between our trend estimates and those published in Schneider and van der A (2012) can be explained by the different reference year (1996 vs. 2002).

The retrieved NO_2 trend is comparable using original and resolution-corrected GOME measurements in the level shift fit; in virtually all cases the absolute growth rates between the two datasets agree within the assumed uncertainty. The respective relative trends, however, differ considerably. This results from the resolution-corrected GOME data in the reference year 1996 having systematically higher NO_2 columns than in the original dataset.

Exemplarily, time series for New York, Tehran, Mumbai, and Beijing are shown in Fig. 17. For all four cities, the

Table 4. Annual growth rate ΔVCD_{trop} NO_2 from the level shift model (Eq. 3) and the multi-instrument fit (Eq. 9) for a list of megacities. The relative trends have been computed relative to the 1996 annual mean. Non-significant trends (see Eq. 6) are shown in italics.

City	Level shift model (orig. GOME data)		Multi-instrument fit	
	$[10^{14}\,\mathrm{molec\,cm^{-2}\,yr^{-1}}]$	$[\%\,\mathrm{yr^{-1}}]$	$[10^{14}\,\mathrm{molec\,cm^{-2}\,yr^{-1}}]$	$[\%\,\mathrm{yr^{-1}}]$
Algiers	$+0.74 \pm 0.14$	$+3.64 \pm 0.69$	$+0.60 \pm 0.18$	$+2.89 \pm 0.87$
Athens	-2.33 ± 0.70	-4.1 ± 1.2	-2.09 ± 0.83	-3.7 ± 1.5
Baghdad	$+3.54 \pm 0.33$	$+20.7 \pm 1.9$	$+3.24 \pm 0.37$	$+18.0 \pm 2.1$
Beijing	$+8.8 \pm 2.5$	$+6.7 \pm 1.9$	$+9.5 \pm 2.9$	$+7.3 \pm 2.2$
Buenos Aires	$+1.14 \pm 0.48$	$+3.9 \pm 1.6$	*$+0.55 \pm 0.51$*	*$+1.7 \pm 1.6$*
Cairo	$+1.91 \pm 0.25$	$+7.21 \pm 0.93$	$+1.73 \pm 0.28$	$+6.4 \pm 1.0$
Chicago	-6.7 ± 1.8	-4.1 ± 1.1	-6.2 ± 2.2	-3.9 ± 1.4
Dhaka	$+3.66 \pm 0.52$	$+27.2 \pm 3.9$	$+3.41 \pm 0.54$	$+24.0 \pm 3.8$
Damascus	$+3.44 \pm 0.54$	$+10.2 \pm 1.6$	$+2.62 \pm 0.53$	$+7.2 \pm 1.4$
Guangzhou	*$+1.2 \pm 2.0$*	*1.3 ± 2.0*	*$+0.2 \pm 2.6$*	*$+0.2 \pm 2.6$*
Hong Kong	*-2.6 ± 1.8*	*-2.3 ± 1.6*	*-1.1 ± 2.3*	*-1.0 ± 2.1*
Istanbul	*-0.5 ± 1.1*	*-0.7 ± 1.5*	*-0.4 ± 1.1*	*-0.5 ± 1.5*
Jakarta	-1.45 ± 0.42	-3.9 ± 1.1	-1.19 ± 0.41	3.3 ± 1.1
Jeddah	$+1.30 \pm 0.29$	$+4.07 \pm 0.92$	$+1.42 \pm 0.36$	$+4.5 \pm 1.2$
Karachi	$+0.94 \pm 0.22$	$+6.8 \pm 1.6$	$+0.85 \pm 0.25$	$+6.0 \pm 1.8$
Kolkata	$+0.75 \pm 0.22$	$+2.98 \pm 0.89$	$+0.80 \pm 0.26$	$+3.2 \pm 1.0$
Lagos	$+0.41 \pm 0.10$	$+3.41 \pm 0.83$	$+0.33 \pm 0.12$	$+2.68 \pm 0.95$
Lima	$+0.99 \pm 0.40$	$+7.1 \pm 2.9$	$+1.06 \pm 0.36$	$+7.9 \pm 2.7$
London	-4.4 ± 1.3	-2.40 ± 0.71	*-3.0 ± 1.6*	*-1.66 ± 0.91*
Los Angeles	-13.7 ± 1.7	-6.00 ± 0.72	-13.2 ± 2.6	-5.8 ± 1.2
Manila	-1.13 ± 0.18	-5.32 ± 0.85	-1.03 ± 0.20	-4.93 ± 0.95
Mexico City	*-0.65 ± 0.83*	*-1.2 ± 1.5*	*$+0.51 \pm 0.82$*	*$+1.0 \pm 1.6$*
Moscow	*-0.2 ± 1.5*	*-0.3 ± 1.9*	*-1.4 ± 1.6*	*-1.6 ± 1.9*
Mumbai	$+0.82 \pm 0.17$	$+4.31 \pm 0.91$	$+0.70 \pm 0.21$	$+3.6 \pm 1.1$
New Delhi	$+3.07 \pm 0.53$	$+9.3 \pm 1.6$	$+2.57 \pm 0.60$	$+7.4 \pm 1.7$
New York	-5.3 ± 1.7	-2.45 ± 0.80	-5.7 ± 2.3	-2.6 ± 1.0
Osaka	-1.94 ± 0.98	-1.74 ± 0.88	-2.54 ± 0.98	-2.23 ± 0.86
Paris	-4.6 ± 2.0	-3.0 ± 1.3	*-5.2 ± 2.5*	*-3.3 ± 1.6*
Riyadh	$+2.01 \pm 0.39$	$+6.7 \pm 1.3$	$+2.05 \pm 0.38$	$+6.9 \pm 1.3$
São Paolo	*$+0.52 \pm 0.46$*	*-1.3 ± 1.2*	*$+0.37 \pm 0.52$*	*$+0.9 \pm 1.3$*
Seoul	*$+0.6 \pm 1.7$*	*0.4 ± 1.1*	*$+1.0 \pm 1.8$*	*$+0.7 \pm 1.2$*
Shanghai	$+11.9 \pm 3.1$	$+12.8 \pm 3.3$	$+9.4 \pm 3.0$	$+9.2 \pm 2.9$
Shenzhen	*-2.4 ± 1.6*	*-1.9 ± 1.3*	*-2.2 ± 1.7*	*-1.8 ± 1.3*
Tehran	$+2.08 \pm 0.68$	$+5.7 \pm 1.9$	$+2.68 \pm 0.93$	$+7.8 \pm 2.7$
Tokyo	-5.2 ± 1.1	-3.61 ± 0.79	-5.4 ± 1.4	-3.77 ± 0.97

gridded VCD_{trop} NO_2 (on a $\frac{1}{16}^\circ \times \frac{1}{16}^\circ$ grid) have been averaged over an area of $1.0^\circ \times 0.5^\circ$ ($1.0^\circ \times 0.75^\circ$ in the case of Mumbai). In all cases, it is clearly visible that (a) there are significant differences between GOME and SCIAMACHY measurements which must not be ignored, and that (b) these differences are being addressed by the level shift method very well. New York shows a strongly decreasing trend of $-5.3 \pm 1.7 \times 10^{14}\,\mathrm{molec\,cm^{-2}\,yr^{-1}}$. This is considerably stronger than the $-0.3 \pm 1.7 \times 10^{14}\,\mathrm{molec\,cm^{-2}\,yr^{-1}}$ reported by van der A et al. (2008) for the 1996–2006 time period. However, one has to note the differences, namely that our study period is five years longer, and that van der A et al. did not account for instrumental differences between GOME and SCIAMACHY measurements. Figure 17 shows that VCD_{trop} measured by SCIAMACHY are significantly higher than those retrieved from GOME measurements, which leads to an underestimation of a downward trend if not accounted for. Tehran, Mumbai, and Beijing all show very pronounced upward trends of $+2.08 \pm 0.68 \times 10^{14}\,\mathrm{molec\,cm^{-2}\,yr^{-1}}$, $+8.2 \pm 1.7 \times 10^{13}\,\mathrm{molec\,cm^{-2}\,yr^{-1}}$, and $+8.8 \pm 2.5 \times 10^{14}\,\mathrm{molec\,cm^{-2}\,yr^{-1}}$, respectively. These results compare well to those reported by van der A et al. (2008), who quote $+2.6 \pm 0.5 \times 10^{14}\,\mathrm{molec\,cm^{-2}\,yr^{-1}}$, $+7 \pm 3 \times 10^{13}\,\mathrm{molec\,cm^{-2}\,yr^{-1}}$, and $+12 \pm 2.9 \times 10^{14}\,\mathrm{molec\,cm^{-2}\,yr^{-1}}$. When we repeat our trend calculation for the 1996–2006 period, the results become similar to those by van der A et al. (2008) both in magnitude and in uncertainty (see the Supplement). Here, we derive trends of $+1.94 \pm 0.82 \times 10^{14}\,\mathrm{molec\,cm^{-2}\,yr^{-1}}$ and $+8.8 \pm 3.6 \times 10^{14}\,\mathrm{molec\,cm^{-2}\,yr^{-1}}$ for Tehran and Beijing,

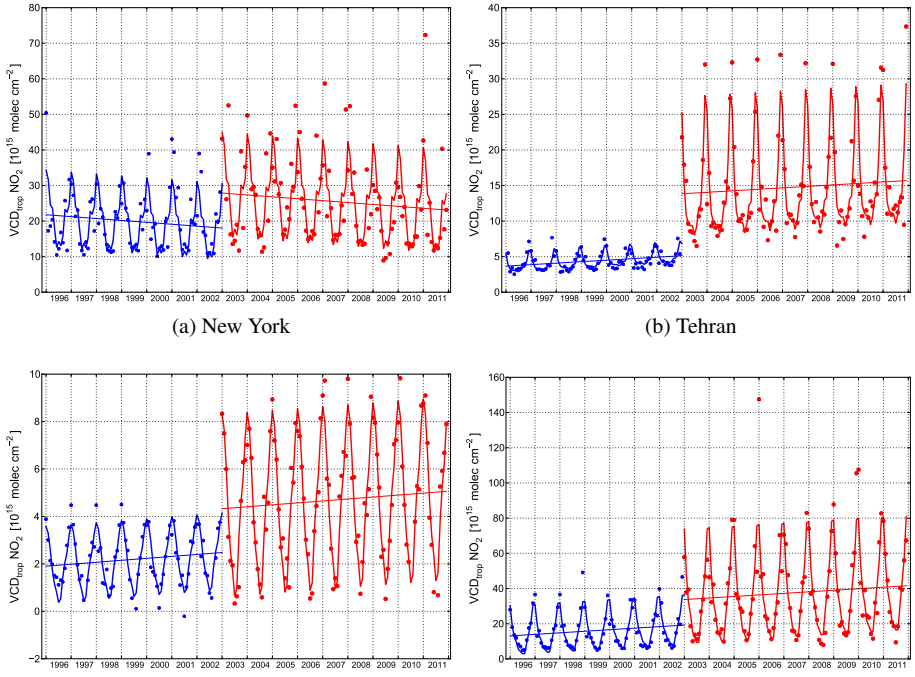

(a) New York (b) Tehran

(c) Mumbai (d) Beijing

Fig. 17. Time series of monthly VCD_{trop} NO_2 (dots), fitted level shift trend model (thick line), and linear component of the fit (straight line) for the time periods 1996–2002 (GOME, blue) and 2003–2011 (SCIAMACHY, red).

respectively. The larger trends by van der A et al. (2008) might partly be caused by them not accounting for the offset between GOME and SCIAMACHY measurements, as the jump in NO_2 values between the two instruments biases a standard trend model towards higher growth rates. Generally, we observe a convincing reduction of the trend uncertainties by using our level shift model, as compared to the estimates presented in van der A et al. (2008), which leads to significant trends in most of the regions considered in this study. However, this reduction in uncertainty is mostly due to the longer study period.

Comparing the trend results from the two study periods 1996–2006 and 1996–2011 further illustrates that, for example, the North American megacities New York and Los Angeles show very pronounced downward NO_2 trends in the longer period, while our trend analysis does not yield any significant trends for 1996-2006 alone. This is due to an interplay between changes in economic activity and emission control measures, which can lead to non-linear NO_2 changes, as already observed by Russell et al. (2012).

In China, it is interesting to note that the cities Guangzhou, Shenzhen, and Hong Kong in south-eastern China do not show significant trends. While this might be expected in Hong Kong, which industrialised earlier and has an advanced level of economic development, it seems unlikely that NO_2 pollution in Shenzhen, whose population has more than doubled since 1995 (O'Donnell, 2011), has not increased. This lack of a detectable trend might be caused by unfavourable temporal sampling, due to high cloud cover, resulting in only very few measurements per month, which leads to large individual uncertainties of the monthly average NO_2 columns, or possibly by some control measures which counteract the emissions from a rapidly increasing population.

6 Combining all four instruments into a level-shift-like trend model

As measurements of tropospheric NO_2 from different satellite instruments are becoming available, it is necessary to find ways to analyse these data in an integrated, consistent and consolidated manner. The level shift model presented in Sect. 5 has the limitation that it can only account for one measurement per time step. Therefore, we evolved the method to be able to use measurements from all four available instruments by developing a trend model accounting for the differences in the measured VCD_{trop} from GOME, SCIAMACHY, OMI, and GOME-2 (Hilboll et al., 2013b).

6.1 Method description

We model the time series $Y(t,i)$ of average NO_2 measurements made by instrument i in month t with the trend model

$$Y(t,i) = \mu_i + \omega t + \eta_i \times \sum_{j=1}^{4} \left(\beta_{1,j} \sin\left(\frac{2\pi j t}{12}\right) + \beta_{2,j} \cos\left(\frac{2\pi j t}{12}\right) \right) + N(t,i). \quad (8)$$

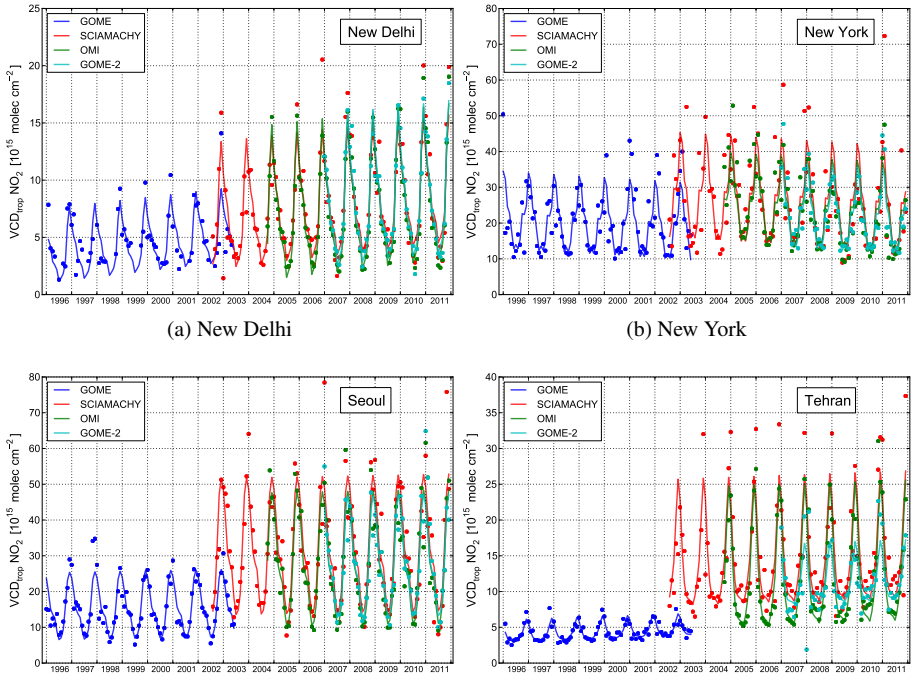

(a) New Delhi (b) New York

(c) Seoul (d) Tehran

Fig. 18. Measured monthly average VCD_{trop} NO_2 (dots) and fitted trend function from the multi-instrument trend model (lines) for the four instruments GOME (blue), SCIAMACHY (red), OMI (green), and GOME-2 (cyan).

ω is the linear trend component, which we assume to be common among all four instruments. μ_i are the offsets of the linear trend per instrument, and η_i gives the relative amplitude of the seasonality component (with $\eta_1 \equiv 1$). The optimal trend estimators $(\hat{\omega}, \ldots)$ are then calculated by minimizing the sum of the squared noise components $N(t,i)$, applying weights to the individual monthly averages $Y(t,i)$ to account for the varying number of instruments providing VCD_{trop} at time t. As a result of the multi-instrument trend model analysing multiple observations per time step, the uncertainties and accurate error estimates of the estimated trends have to be determined using a bootstrap technique. Here, we follow the method detailed in Mudelsee (2010). For each individual time series, we determine the optimal bootstrapping block length using the approach developed by Bühlmann and Künsch (1999). Then we calculate the standard error of the trend estimator $\hat{\omega}$ using the moving block bootstrap with 2000 iterations (Mudelsee, 2010). Finally, we calculate 95 % bootstrap bias-corrected and accelerated confidence intervals for $\hat{\omega}$ (Mudelsee, 2010). We call a trend significant if and only if the confidence interval does not include 0.0.

6.2 Results and discussion

As is apparent from Tables 3 and 4, the linear trend estimates $\hat{\omega}$ from the multi-instrument fit generally agree very well with those derived from the level shift model.

Many regions do not show large differences between the instruments (e.g. New Delhi), while in other regions these differences are strongly pronounced, as in Tehran (see Fig. 18). Reasons for this include differing spatial distributions of both the NO_2 columns themselves and other factors influencing the NO_2 retrieval, such as aerosol load, surface altitude, and surface spectral reflectance. All these quantities influence the retrieved NO_2 columns, as the differing spatial resolutions of the satellite measurements lead to instrument-dependent spatial sampling, which in turn has a significant effect on the observed NO_2 amounts or levels and their seasonality. A further issue is the different local times of the satellite measurements. As OMI measures in the early afternoon, the diurnal cycles of NO_2 and aerosols, as well as the different angular sampling of spectral surface reflectance, can lead to offsets between the instruments.

This can result in varying ground amounts of retrieved NO_2 columns and varying seasonal cycles between the four instruments. For large ground scenes, the NO_2 columns will be more inhomogeneous than for small ones, leading to a stronger smearing of the high pollution peaks of, e.g., megacities. We show this exemplarily for the three cities New Delhi, New York, and Tehran, using topography (Hastings et al., 1998), population density (CIESIN, IFPRI, the World Bank, and CIAT, 2011), and NO_x emission (European Commission, JRC and PBL, 2011) data (see Fig. 19). In New Delhi, which lies in a topographically flat region with homogeneously high population density and NO_x emissions,

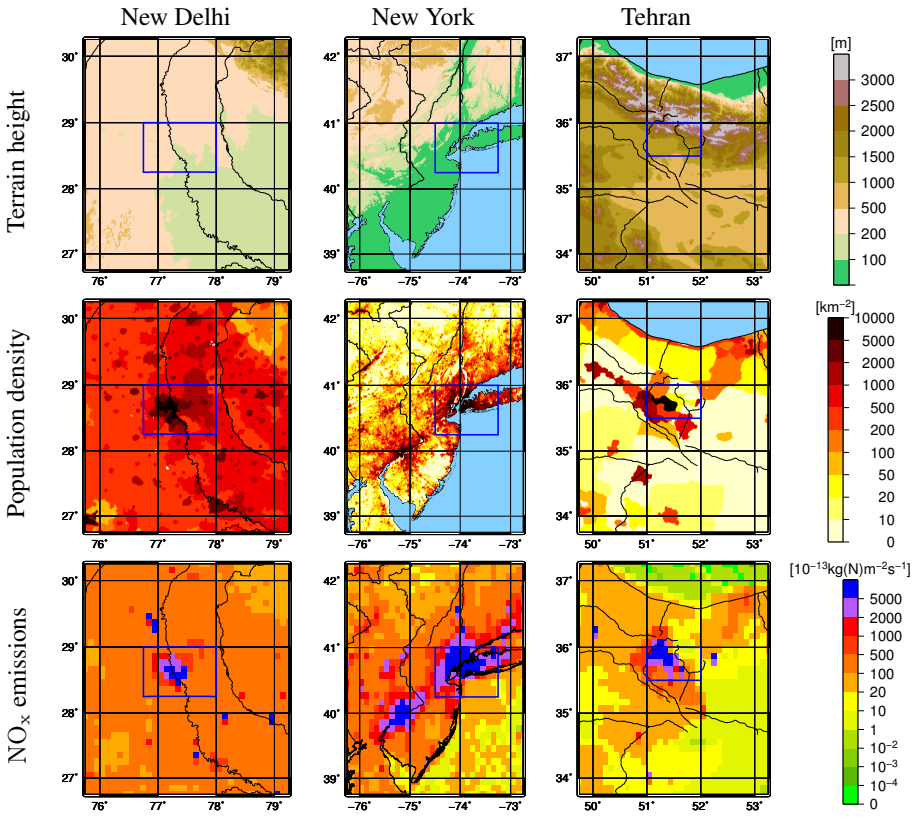

Fig. 19. Topography, population density, and NO_x emissions for the three selected megacity regions New Delhi (India), New York (United States), and Tehran (Iran). Topographic data is from the GLOBE project (Hastings et al., 1998), population density data from the GRUMP dataset (CIESIN, IFPRI, the World Bank, and CIAT, 2011), and NO_x emission values are from the EDGAR database (European Commission, JRC and PBL, 2011).

virtually no difference between the four instruments can be observed. Under these conditions, NO_2 can spread without barriers. The area around New York City is also topographically flat, but the NO_x emissions are mostly constrained to land, with the exception of shipping routes and aircraft corridors, land accounting for only $\frac{2}{3}$ of the whole area. Therefore, emitted NO_2 can spread towards the ocean, leading to NO_2 column gradients within the observed area. This NO_2 gradient between megacity and open ocean leads to the noticeable impact of the instruments' pixel size on retrieved VCD_{trop} values. In the case of Tehran, emissions are mostly confined to the city's boundaries. Moreover, the emitted NO_2 cannot spread evenly throughout the area, because Tehran is bordered by the Alborz mountain range towards the north and east, leading to inhomogeneous NO_2 pollution in the observed area and thus to lower NO_2 columns in the case of large pixel sizes. Therefore, the NO_2 time series over Tehran show a very strong dependence on the instrument's spatial resolution.

The multi-instrument trend model presented in this section has the advantage of being suitable for the later inclusion of measurements from future satellite instruments. Under the assumption that the growth rate of the linear trend component is constant among all instruments, the model is therefore an excellent tool to assess the temporal evolution of the measured quantity. In the trend calculation, each month has the same weight, while at the same time a maximum of the available measurement data is included in the fitting procedure, and instrumental differences are accounted for to some extent.

6.3 Extensions to the multi-instrument trend model

As a result of the multitude of factors contributing to the magnitude and changes in tropospheric NO_2 column densities, it is well possible that change rates are not constant throughout the seasons. An example are changes in the relative importance of emission sources with large seasonality (heating) and others which are rather constant (transportation). One way to account for this is to link temporal changes to the amplitude of the seasonality component of Eq. (9). The effect of such a model extension requires the introduction of a parameter ξ representing the rate of change of the seasonality component:

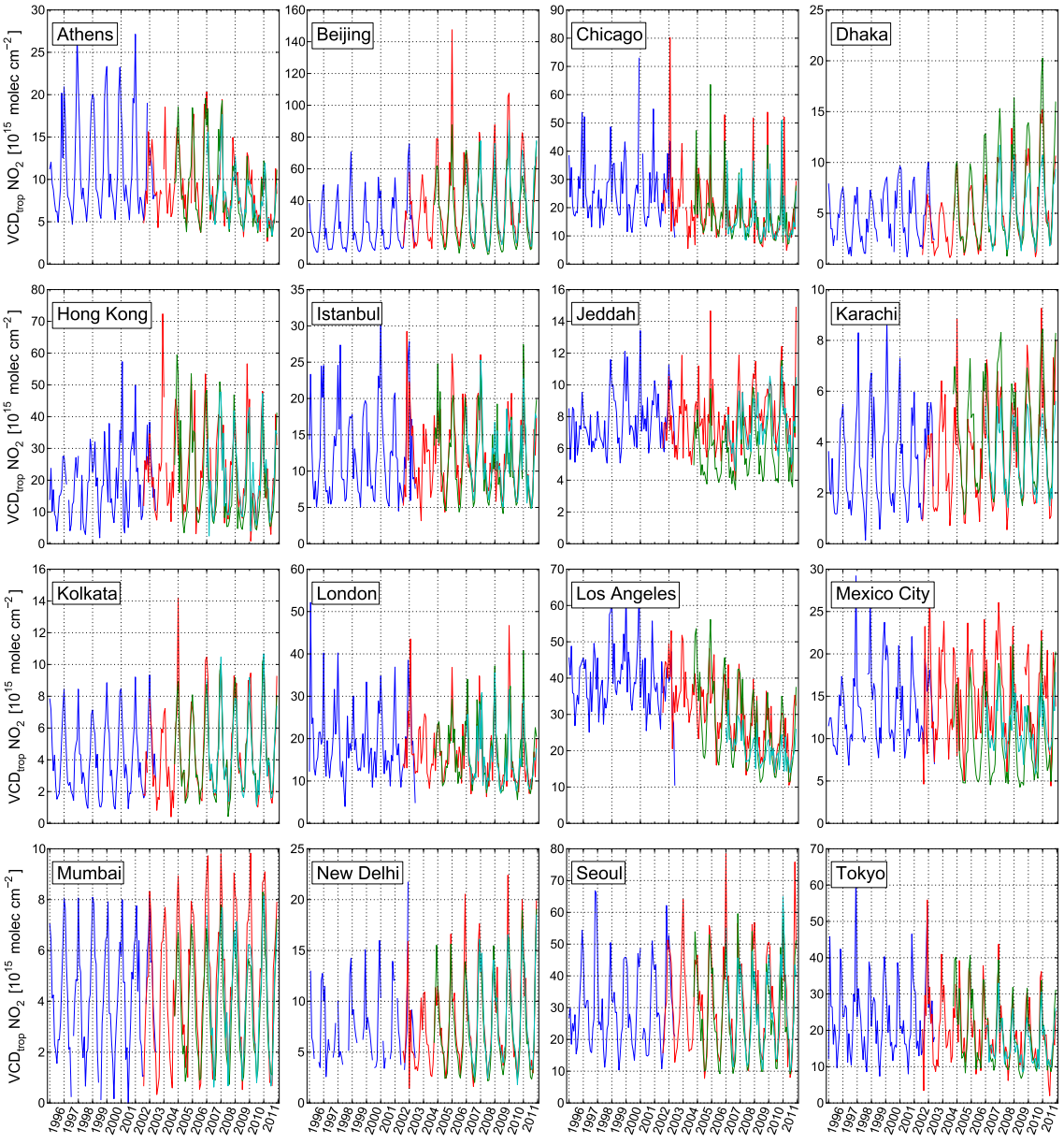

Fig. 20. Time series of monthly mean VCD_{trop} NO_2 from GOME (blue), SCIAMACHY (red), OMI (green), and GOME-2 (cyan). The GOME measurements have been corrected for the instrument's pixel size using the mechanism presented in Sect. 4.

$$Y_i(t,i) = \mu_i + \omega t + (1+\xi t) \times \eta_i \times \sum_{j=1}^{4} \left(\beta_{1,j} \sin\left(\frac{2\pi j t}{12}\right) + \beta_{2,j} \cos\left(\frac{2\pi j t}{12}\right)\right) + N(t,i). \quad (9)$$

The resulting trend estimators are shown in the Supplement. We find that the trend estimator $\hat{\omega}$ is of smaller magnitude than when the seasonality is kept at a fixed amplitude. The increasing (decreasing) NO_2 values are partly absorbed by a changing amplitude of the seasonality signal, which in turn leads to lower linear trend estimators $\hat{\omega}$.

In virtually all cases the signs of the linear and harmonic trend estimators $\hat{\omega}$ and $\hat{\xi}$ coincide. The observed magnitude of $\hat{\xi}$ however varies widely, depending on the region of interest. While for many regions the two estimators are similar in (relative) magnitude (e.g. Beijing, Hong Kong, New York, Po Valley), often the harmonic component $\hat{\xi}$ is significantly larger than $\hat{\omega}$, as, e.g., in Athens, Baghdad, Barcelona, and Cairo. As summer NO_2 values often show slower rates of change than winter values, this is averaged out when assessing the linear growth rates. The seasonal cycle however is strengthened by this effect, as the difference between summer and winter values becomes larger.

In a further step, the trend model should be extended to account for the different noise levels of the individual

instruments' time series. This is common in climate time series analysis (see Mudelsee, 2010) and assures that instruments with more stable measurements have more weight in the fitting process. Usually, this is achieved by minimizing the variability-weighted squared noise components $\frac{N(t,i)}{S(i)}$, where $S(i)$ denotes the standard deviation of all measurements of instrument i. In practice, this common correction leads to a slight reduction of the retrieved linear trend estimates for many regions. As a result of the relatively high variability of SCIAMACHY measurements (when compared to OMI and GOME-2, mostly caused by the significantly lower spatial and temporal coverage), the instrument has lower relative weight in the trend calculation. Since most regions show the strongest relative NO_2 changes for SCIAMACHY observations (see, e.g. Fig. 20), the instrument's lower relative weight thus leads to a slight reduction of the calculated trend estimates. For the results shown in Tables 3 and 4, we do not apply this correction so as to make the results more comparable to those retrieved from the resolution correction factor and level shift methods.

7 Summary and conclusions

In the present study, we investigate the temporal evolution of tropospheric NO_2 columns retrieved from satellite observations during the 1996–2011 time period. For the first time, the instrumental difference in ground pixel size between the used satellite sensors has been explicitly accounted for. To assess the robustness of this approach and the reliability of the derived linear changes or trends, we introduced two additional complementary strategies for the derivation of instrumental and multiple instrumental trends in tropospheric NO_2.

Firstly, we spatially averaged SCIAMACHY spectra to be comparable in ground pixel size to GOME measurements, performed DOAS fits on these spectra, and calculated a resolution correction factor from these down-scaled and the regular SCIAMACHY measurements. These correction factors were shown to represent the spatial distribution of the NO_2 signal measured at a given point on the earth, as they very well repeat the patterns observed in NO_x emissions. The GOME measurements were then multiplied with these correction factors. While this can lead to an over-correction in some cases, we showed that generally, the corrected NO_2 time series from GOME measurements over individual city regions are brought into very good agreement with SCIAMACHY values during the time period of parallel measurements, facilitating trend analyses on a spatial resolution appropriate for SCIAMACHY observations.

Secondly, we applied a trend model similar to that developed by Mieruch et al. (2008) for the study of H_2O trends to the combined GOME/SCIAMACHY NO_2 time series, which explicitly accounts for a spatially varying additive offset between the two instruments. The spatial pattern of these offsets was shown to be very similar to that of the resolution correction factor.

We calculated annual change rates in tropospheric NO_2 columns for a number of large urban agglomerations (see Table 4). Compared to previous studies, our results show considerably lower uncertainties of the retrieved trend estimates, most probably due to the longer study period of 1996–2011. This model was then evolved to be able to include measurements from GOME-2 and OMI, and to account for a trend in the amplitude of the seasonal cycle.

The results show for the period of observation that NO_2 columns over the industrialised countries (US, Europe, Japan, Australia) have been steadily decreasing, with significant trends of up to $-6\,\%\,\mathrm{yr}^{-1}$. On the other hand, Chinese and Indian megacities, as well as many urban centres in the Middle East, show very strong upward trends of up to $+20\,\%\,\mathrm{yr}^{-1}$. Trends calculated with data from all four instruments agree well with those derived from GOME and SCIAMACHY measurements alone, highlighting the consistency of the satellite observations in spite of differences in sampling, spatial resolution, and overpass time. On the other hand, trends derived from the GOME and SCIAMACHY time series independently show systematic differences. These are attributed to changes in emission trends between the two time periods, e.g. the accelerated development in China or the recent emission reductions in the US due to improved technology and economic crises.

These strong and significant changes in tropospheric NO_2 columns over megacities show the ongoing need for further instruments which are able to continue appropriate measurements. When assessing the temporal evolution, it is imperative that instrumental differences are considered. This is especially true for the upcoming Sentinel-5 Precursor mission, as the proposed TROPOMI instrument will have a very high spatial resolution of $7 \times 7\,\mathrm{km}^2$ (Veefkind et al., 2012). With the increasing length of the NO_2 time series available for analysis, the potential to understand the relationship between NO_2 emissions and their atmospheric abundances becomes better than ever.

Appendix A

We show the "raw" NO_2 measurements from GOME (resolution-corrected), SCIAMACHY, OMI, and GOME-2 for some selected megacity regions in Fig. 20. Several interesting features can be observed from these plots. In Athens, for example, NO_2 columns seem to be increasing until about 2004, followed by some years of stagnation, which turn into a rapid downward trend 2008/2009 (Vrekoussis et al., 2013). This is attributed to the deep economic crisis affecting Greece since that time. Similarly, Chicago and Los Angeles both see downward trends, starting from stagnating and even increasing NO_2 columns before 2000, and

leading to significant NO_2 decreases in following years, with the most recent years showing some sign of slowdown of the decreases. This can be attributed to both increasingly efficient emission control measures and a slowdown of economic activity, as has been reported by Russell et al. (2012).

In Beijing, summer minima in 2008 are clearly lower than in the preceding and following years. This effect has been linked to the 2008 summer Olympic Games and has been studied, e.g. by Mijling et al. (2009). Over Jeddah and Mexico City, the NO_2 columns derived from the OMI instrument are significantly lower than those from SCIAMACHY and GOME-2, especially during the summer minima. This might be an effect of the different measurement time, as OMI measures in the early afternoon as opposed to the morning for all other instruments. For Mexico City, Zhang et al. (2009b) studied the diurnal cycle of NO_2 surface concentrations, and showed that 10:00 LT morning values were about three times higher than 13:45 LT values.

Supplementary material related to this article is available online at: http://www.atmos-chem-phys.net/13/4145/2013/acp-13-4145-2013-supplement.pdf.

Acknowledgements. Andreas Hilboll gratefully acknowledges funding by the "Earth System Science Research School (ESSReS)", an initiative of the Helmholtz Association of German research centres (HGF) at the Alfred Wegener Institute for Polar and Marine Research. The authors would like to acknowledge the European Union Seventh Framework Programme (FP7/2007–2013) project CityZen (Grant Agreement no. 212095). Parts of this work were funded by the State of Bremen and the University of Bremen. Jan Aschmann and Nadine Wieters proved extremely helpful in setting up the B3dCTM model. The authors are grateful to Sebastian Mieruch, Manfred Mudelsee, and Igor Konovalov for valuable discussions on time series analysis, and thank Joana Leitão for giving valuable recommendations regarding the manuscript. Greet Maenhout from JRC proved very helpful in fixing the EDGAR emission database for 2008. GOME and SCIAMACHY radiances have been provided by ESA. OMI Level-2 data used in this study were acquired as part of the activities of NASA's Science Mission Directorate, and are archived and distributed by the Goddard Earth Sciences (GES) Data and Information Services Center (DISC). GOME-2/Metop-A Level-1 data have been provided by EUMETSAT. ECMWF ERA-Interim data were supplied by the "European Centre for Medium-Range Weather Forecasts" at Reading, UK. The authors thank two anonymous referees for their valuable comments. The service charges for this open access publication have been partially covered by the Deutsche Forschungsgemeinschaft (DFG).

Edited by: I. Aben

References

Beirle, S., Platt, U., Wenig, M., and Wagner, T.: Highly resolved global distribution of tropospheric NO_2 using GOME narrow swath mode data, Atmos. Chem. Phys., 4, 1913–1924, doi:10.5194/acp-4-1913-2004, 2004.

Boersma, K. F., Eskes, H. J., and Brinksma, E. J.: Error analysis for tropospheric NO_2 retrieval from space, J. Geophys. Res., 109, D04311, doi:10.1029/2003JD003962, 2004.

Boersma, K. F., Eskes, H. J., Veefkind, J. P., Brinksma, E. J., van der A, R. J., Sneep, M., van den Oord, G. H. J., Levelt, P. F., Stammes, P., Gleason, J. F., and Bucsela, E. J.: Near-real time retrieval of tropospheric NO_2 from OMI, Atmos. Chem. Phys., 7, 2103–2118, doi:10.5194/acp-7-2103-2007, 2007.

Bogumil, K., Orphal, J., Homann, T., Voigt, S., Spietz, P., Fleischmann, O., Vogel, A., Hartmann, M., Kromminga, H., Bovensmann, H., Frerick, J., and Burrows, J. P.: Measurements of molecular absorption spectra with the SCIAMACHY preflight model: instrument characterization and reference data for atmospheric remote-sensing in the 230–2380 nm region, J. Photochem. Photobiol. A, 157, 167–184, doi:10.1016/S1010-6030(03)00062-5, 2003.

Bovensmann, H., Burrows, J. P., Buchwitz, M., Frerick, F., Noël, S., and Rozanov, V. V.: SCIAMACHY: mission objectives and measurement modes, J. Atmos. Sci., 56, 127–150, doi:10.1175/1520-0469(1999)056<0127:SMOAMM>2.0.CO;2, 1999.

Bühlmann, P. and Künsch, H. R.: Block length selection in the bootstrap for time series, Comput. Stat. Data Analys., 31, 295–310, doi:10.1016/S0167-9473(99)00014-6, 1999.

Burrows, J. P., Hölzle, E., Goede, A., Visser, H., and Fricke, W.: SCIAMACHY - scanning imaging absorption spectrometer for atmospheric chartography, Acta Astronaut., 35, 445–451, doi:10.1016/0094-5765(94)00278-T, 1995.

Burrows, J. P., Weber, M., Buchwitz, M., Rozanov, V. V., Ladstätter-Weißenmayer, A., Richter, A., DeBeek, R., Hoogen, R., Bramstedt, K., Eichmann, K.-U., and Eisinger, M.: The Global Ozone Monitoring Experiment (GOME): mission concept and first scientific results, J. Atmos. Sci., 56, 151–175, doi:10.1175/1520-0469(1999)056<0151:TGOMEG>2.0.CO;2, 1999.

Burrows, J. P., Platt, U., and Borrell, P.: The Remote Sensing of Tropospheric Composition from Space, 1st Edn., Springer, Heidelberg, Germany, 2011.

Callies, J., Corpaccioli, E., Eisinger, M., Hahne, A., and Lefebvre, A.: GOME-2 – Metop's second-generation sensor for operational ozone monitoring, ESA Bull.-Eur. Space, 102, 28–36, 2000.

Castellanos, P. and Boersma, K. F.: Reductions in nitrogen oxides over Europe driven by environmental policy and economic recession, Sci. Reports, 2, 265, doi:10.1038/srep00265, 2012.

Center for International Earth Science Information Network (CIESIN), Columbia University, International Food Policy Research Institute (IFPRI), the World Bank, and Centro Internacional de Agricultura Tropical (CIAT): Global Rural-Urban Mapping Project, Version 1 (GRUMPv1): Population density grid, Socioeconomic Data and Applications Center (SEDAC), Columbia University, Palisades, NY, USA, 2011.

Chance, K.: Analysis of BrO measurements from the Global Ozone Monitoring Experiment, Geophys. Res. Lett., 25, 3335–3338, doi:10.1029/98GL52359, 1998.

de Ruyter de Wildt, M., Eskes, H., and Boersma, K. F.: The global economic cycle and satellite-derived NO_2 trends over shipping lanes, Geophys. Res. Lett., 39, 2–7, doi:10.1029/2011GL049541, 2012.

European Commission, Joint Research Centre (JRC) and Netherlands Environmental Assessment Agency (PBL): Emission Database for Global Atmospheric Research (EDGAR), http://edgar.jrc.ec.europa.eu (last access: 12 August 2012), 2011.

Finlayson-Pitts, B. and Pitts Jr., J. N.: Chemistry of the Upper and Lower Atmosphere: Theory, Experiments, and Applications, 6th Edn., Academic Press, San Diego, CA, USA, 1999.

Franke, K., Richter, A., Bovensmann, H., Eyring, V., Jöckel, P., Hoor, P., and Burrows, J. P.: Ship emitted NO_2 in the Indian Ocean: comparison of model results with satellite data, Atmos. Chem. Phys., 9, 7289–7301, doi:10.5194/acp-9-7289-2009, 2009.

Ghude, S. D., Fadnavis, S., Beig, G., Polade, S. D., and van der A, R. J.: Detection of surface emission hot spots, trends, and seasonal cycle from satellite-retrieved NO_2 over India, J. Geophys. Res., 113, 13 pp., D20305, doi:10.1029/2007JD009615, 2008.

Gottwald, M. and Bovensmann, H.: SCIAMACHY – Exploring the Changing Earth's Atmosphere, Springer Netherlands, Dordrecht, 2011.

Granier, C., Bessagnet, B., Bond, T., D'Angiola, A., Denier van der Gon, H., Frost, G. J., Heil, A., Kaiser, J. W., Kinne, S., Klimont, Z., Kloster, S., Lamarque, J.-F., Liousse, C., Masui, T., Meleux, F., Mieville, A., Ohara, T., Raut, J.-C., Riahi, K., Schultz, M. G., Smith, S. J., Thompson, A., Aardenne, J., Werf, G. R., and Vuuren, D. P.: Evolution of anthropogenic and biomass burning emissions of air pollutants at global and regional scales during the 1980–2010 period, Clim. Change, 109, 163–190, doi:10.1007/s10584-011-0154-1, 2011.

Greenblatt, G. D., Orlando, J. J., Burkholder, J. B., and Ravishankara, A. R.: Absorption measurements of oxygen between 330 and 1140 nm, J. Geophys. Res., 95, 18577–18582, doi:10.1029/JD095iD11p18577, 1990.

Hastings, D. A., Dunbar, P. K., Elphingstone, G. M., Bootz, M., Murakami, H., Holland, P., Bryant, N. A., Logan, T. L., Muller, J.-P., Schreier, G., and MacDonald, J. S.: The Global Land One-kilometer Base Elevation (GLOBE) Digital Elevation Model, Version 1.0, National Oceanic and Atmospheric Administration, Boulder, CO, USA, 1998.

Hayn, M., Beirle, S., Hamprecht, F. A., Platt, U., Menze, B. H., and Wagner, T.: Analysing spatio-temporal patterns of the global NO2-distribution retrieved from GOME satellite observations using a generalized additive model, Atmos. Chem. Phys., 9, 6459–6477, doi:10.5194/acp-9-6459-2009, 2009.

He, Y., Uno, I., Wang, Z., Ohara, T., Sugimoto, N., Shimizu, A., Richter, A., and Burrows, J. P.: Variations of the increasing trend of tropospheric NO_2 over central east China during the past decade, Atmos. Environ., 41, 4865–4876, doi:10.1016/j.atmosenv.2007.02.009, 2007.

Hilboll, A., Richter, A., Rozanov, A., Hodnebrog, Ø., Heckel, A., Solberg, S., Stordal, F., and Burrows, J. P.: Improvements to the retrieval of tropospheric NO_2 from satellite – stratospheric correction using SCIAMACHY limb/nadir matching and comparison to Oslo CTM2 simulations, Atmos. Meas. Tech., 6, 565–584, doi:10.5194/amt-6-565-2013, 2013a.

Hilboll, A., Richter, A., and Burrows, J. P.: NO_2 pollution trends over megacities 1996–2010 from combined multiple satellite data sets, in: Earth System Sciences: Bridging the Gaps between Disciplines. A Multi-Disciplinary Helmholtz Graduate Research School, edited by: Lohmann, G., Wolf-Gladrow, D., Notholt, J., Unnithan, V., Grosfeld, K., and Wegner, A., Springer, Heidelberg, 9–15, 2013b.

Horowitz, L. W., Walters, S., Mauzerall, D. L., Emmons, L. K., Rasch, P. J., Granier, C., Tie, X., Lamarque, J.-F., Schultz, M. G., Tyndall, G. S., Orlando, J. J., and Brasseur, G. P.: A global simulation of tropospheric ozone and related tracers: description and evaluation of MOZART, version 2, J. Geophys. Res., 108, 25 pp., 4784, doi:10.1029/2002JD002853, 2003.

Irie, H., Sudo, K., Akimoto, H., Richter, A., Burrows, J. P., Wagner, T., Wenig, M. O., Beirle, S., Kondo, Y., Sinyakov, V. P., and Goutail, F.: Evaluation of long-term tropospheric NO_2 data obtained by GOME over East Asia in 1996–2002, Geophys. Res. Lett., 32, 2–5, doi:10.1029/2005GL022770, 2005.

Kim, S.-W., Heckel, A., McKeen, S. A., Frost, G. J., Hsie, E.-Y., Trainer, M. K., Richter, A., Burrows, J. P., Peckham, S. E., and Grell, G. A.: Satellite-observed US power plant NO_X emission reductions and their impact on air quality, Geophys. Res. Lett., 33, 5 pp., L22812, doi:10.1029/2006GL027749, 2006.

Koelemeijer, R. B. A., de Haan, J. F., and Stammes, P.: A database of spectral surface reflectivity in the range 335–772 nm derived from 5.5 years of GOME observations, J. Geophys. Res., 108, 4070, doi:10.1029/2002JD002429, 2003.

Konovalov, I. B., Beekmann, M., Richter, A., and Burrows, J. P.: Inverse modelling of the spatial distribution of NO_X emissions on a continental scale using satellite data, Atmos. Chem. Phys., 6, 1747–1770, doi:10.5194/acp-6-1747-2006, 2006.

Konovalov, I. B., Beekmann, M., Richter, A., Burrows, J. P., and Hilboll, A.: Multi-annual changes of NO_X emissions in megacity regions: nonlinear trend analysis of satellite measurement based estimates, Atmos. Chem. Phys., 10, 8481–8498, doi:10.5194/acp-10-8481-2010, 2010.

Lamsal, L. N., Martin, R. V., Padmanabhan, A., Donkelaar, A. V., Zhang, Q., Sioris, C. E., Chance, K., Kurosu, T. P., and Newchurch, M. J.: Application of satellite observations for timely updates to global anthropogenic NO_X emission inventories, Geophys. Res. Lett., 38, L05810, doi:10.1029/2010GL046476, 2011.

Leue, C., Wenig, M. O., Wagner, T., Klimm, O., Platt, U., and Jähne, B.: Quantitative analysis of NO_X emissions from Global Ozone Monitoring Experiment satellite image sequences, J. Geophys. Res., 106, 5493–5505, doi:10.1029/2000JD900572, 2001.

Levelt, P., van den Oord, G., Dobber, M., Malkki, A., Visser, H., de Vries, J., Stammes, P., Lundell, J., and Saari, H.: The ozone monitoring instrument, IEEE T. Geosci. Remote, 44, 1093–1101, doi:10.1109/TGRS.2006.872333, 2006.

Lin, J.-T. and McElroy, M. B.: Detection from space of a reduction in anthropogenic emissions of nitrogen oxides during the Chinese economic downturn, Atmos. Chem. Phys., 11, 8171–8188, doi:10.5194/acp-11-8171-2011, 2011.

Martin, R. V., Chance, K., Jacob, D. J., Kurosu, T. P., Spurr, R. J. D., Bucsela, E., Gleason, J. F., Palmer, P. I., Bey, I., Fiore, A. M., Li, Q., Yantosca, R. M., and Koelemeijer, R. B. A.: An improved retrieval of tropospheric nitrogen dioxide from GOME, J. Geophys. Res., 107, 4437, doi:10.1029/2001JD001027, 2002.

Mieruch, S., Noël, S., Bovensmann, H., and Burrows, J. P.: Analysis of global water vapour trends from satellite measurements in the visible spectral range, Atmos. Chem. Phys., 8, 491–504, doi:10.5194/acp-8-491-2008, 2008.

Mijling, B., van der A, R. J., Boersma, K. F., Roozendael, M. V., Smedt, I. D., and Kelder, H. M.: Reductions of NO_2 detected from space during the 2008 Beijing Olympic Games, Geophys. Res. Lett., 36, L13801, doi:10.1029/2009GL038943, 2009.

Molina, M. J. and Molina, L. T.: Megacities and atmospheric pollution, J. Air Waste Manag. Assoc., 54, 644–680, 2004.

Mudelsee, M.: Climate Time Series Analysis, Atmospheric and Oceanographic Sciences Library, no. 42, Springer, Dordrecht, the Netherlands, 2010.

Noxon, J. F.: Atmospheric nitrogen fixation by lightning, Geophys. Res. Lett., 3, 463–465, doi:10.1029/GL003i008p00463, 1976.

Noxon, J. F.: Tropospheric NO_2, J. Geophys. Res., 83, 3051–3057, doi:10.1029/JC083iC06p03051, 1978.

Nüß, J. H.: Improvements of the retrieval of tropospheric NO_2 from GOME and SCIAMACHY data, PhD thesis, Universität Bremen, Bremen, Germany, 2005.

O'Donnell, M. A.: Shenzhen population statistics, 1979–2011, available at: https://maryannodonnell.wordpress.com/2011/09/10/shenzhen-population-statistics-1979-2011/ (12 September 2012), 2011.

Platt, U. and Stutz, J.: Differential Optical Absorption Spectroscopy, Physics of Earth and Space Environments, Springer, Berlin, Germany, 2008.

Richter, A. and Burrows, J. P.: Tropospheric NO_2 from GOME measurements, Adv. Space Sci., 29, 1673–1683, doi:10.1016/S0273-1177(02)00100-X, 2002.

Richter, A., Eyring, V., Burrows, J. P., Bovensmann, H., Lauer, A., Sierk, B., and Crutzen, P. J.: Satellite measurements of NO_2 from international shipping emissions, Geophys. Res. Lett., 31, L23110, doi:10.1029/2004GL020822, 2004.

Richter, A., Burrows, J. P., Nüß, H., Granier, C., and Niemeier, U.: Increase in tropospheric nitrogen dioxide over China observed from space, Nature, 437, 129–132, doi:10.1038/nature04092, 2005.

Richter, A., Begoin, M., Hilboll, A., and Burrows, J. P.: An improved NO_2 retrieval for the GOME-2 satellite instrument, Atmos. Meas. Tech., 4, 1147–1159, doi:10.5194/amt-4-1147-2011, 2011.

Rothman, L., Gamache, R., Tipping, R., Rinsland, C., Smith, M., Benner, D., Devi, V., Flaud, J.-M., Camy-Peyret, C., Perrin, A., Goldman, A., Massie, S., Brown, L., and Toth, R.: The HITRAN molecular database: editions of 1991 and 1992, J. Quant. Spectrosc. Ra., 48, 469–507, doi:10.1016/0022-4073(92)90115-K, 1992.

Rozanov, A., Rozanov, V. V., Buchwitz, M., Kokhanovsky, A. A., and Burrows, J. P.: SCIATRAN 2.0 – a new radiative transfer model for geophysical applications in the 175–2400 nm spectral region, Adv. Space Sci., 36, 1015–1019, doi:10.1016/j.asr.2005.03.012, 2005.

Russell, A. R., Valin, L. C., and Cohen, R. C.: Trends in OMI NO_2 observations over the United States: effects of emission control technology and the economic recession, Atmos. Chem. Phys., 12, 12197–12209, doi:10.5194/acp-12-12197-2012, 2012.

Schneider, P. and van der A, R. J.: A global single-sensor analysis of 2002–2011 tropospheric nitrogen dioxide trends observed from space, J. Geophys. Res., 117, D16309, doi:10.1029/2012JD017571, 2012.

Seiler, W. and Crutzen, P. J.: Estimates of gross and net fluxes of carbon between the biosphere and the atmosphere from biomass burning, Clim. Change, 2, 207–247, doi:10.1007/BF00137988, 1980.

Sitnov, S. A.: Analysis of spatial-temporal variability of tropospheric NO_2 column over Moscow megapolis using OMI spectrometer (Aura satellite) data, Dokl. Earth Sci., 429, 1511–1517, doi:10.1134/S1028334X09090219, 2010.

Stavrakou, T., Müller, J.-F., Boersma, K. F., de Smedt, I., and van der A, R. J.: Assessing the distribution and growth rates of NO_x emission sources by inverting a 10-year record of NO_2 satellite columns, Geophys. Res. Lett., 35, L10801, doi:10.1029/2008GL033521, 2008.

Tiao, G. C., Reinsel, G. C., Xu, D., Pedrick, J. H., Zhu, X., Miller, A. J., DeLuisi, J. J., Mateer, C. L., and Wuebbles, D. J.: Effects of autocorrelation and temporal sampling schemes on estimates of trend and spatial correlation, J. Geophys. Res., 95, 20507–20517, doi:10.1029/JD095iD12p20507, 1990.

United Nations, Department of Economic and Social Affairs, Population Division: World Urbanization Prospects, the 2011 Revision Highlights, Tech. rep., New York, USA, 2012.

van der A, R. J., Eskes, H. J., Boersma, K. F., van Noije, T. P. C., van Roozendael, M., de Smedt, I., Peters, D. H. M. U., and Meijer, E. W.: Trends, seasonal variability and dominant NO_x source derived from a ten year record of NO_2 measured from space, J. Geophys. Res., 113, D04302, doi:10.1029/2007JD009021, 2008.

Veefkind, J., Aben, I., McMullan, K., Förster, H., de Vries, J., Otter, G., Claas, J., Eskes, H., de Haan, J., Kleipool, Q., van Weele, M., Hasekamp, O., Hoogeveen, R., Landgraf, J., Snel, R., Tol, P., Ingmann, P., Voors, R., Kruizinga, B., Vink, R., Visser, H., and Levelt, P.: TROPOMI on the ESA Sentinel-5 Precursor: A GMES mission for global observations of the atmospheric composition for climate, air quality and ozone layer applications, Remote Sens. Environ., 120, 70–83, doi:10.1016/j.rse.2011.09.027, 2012.

Voulgarakis, A., Savage, N. H., Wild, O., Braesicke, P., Young, P. J., Carver, G. D., and Pyle, J. A.: Interannual variability of tropospheric composition: the influence of changes in emissions, meteorology and clouds, Atmos. Chem. Phys., 10, 2491–2506, doi:10.5194/acp-10-2491-2010, 2010.

Vountas, M., Rozanov, V. V., and Burrows, J. P.: Ring effect: impact of rotational Raman scattering on radiative transfer in Earth's atmosphere, J. Quant. Spectrosc. Ra., 60, 943–961, doi:10.1016/S0022-4073(97)00186-6, 1998.

Vrekoussis, M., Richter, A., Hilboll, A., Burrows, J. P., Gerasopoulos, E., Lelieveld, J., Barrie, L., Zerefos, C., and Mihalopoulos, N.: Economic Crisis Detected from Space: Air Quality observations over Athens/Greece, Geophys. Res. Lett., 40, 458–463, doi:10.1002/grl.50118, 2013.

Wang, P., Stammes, P., van der A, R., Pinardi, G., and van Roozendael, M.: FRESCO+: an improved O_2 A-band cloud retrieval algorithm for tropospheric trace gas retrievals, Atmos. Chem. Phys., 8, 6565–6576, doi:10.5194/acp-8-6565-2008, 2008.

Weatherhead, E. C., Reinsel, G. C., Tiao, G. C., Meng, X.-L., Choi, D., Cheang, W.-K., Keller, T., DeLuisi, J., Wuebbles, D. J., Kerr, J. B., Miller, A. J., Oltmans, S. J., and Frederick, J. E.: Factors affecting the detection of trends: statistical considerations

and applications to environmental data, J. Geophys. Res., 103, 17149–17161, doi:10.1029/98JD00995, 1998.

Williams, E. J., Hutchinson, G. L., and Fehsenfeld, F. C.: NO_x and N_2O emissions from soil, Global Biogeochem. Cy., 6, 351–388, doi:10.1029/92GB02124, 1992.

World Health Organization: Health Aspects of Air Pollution with Particulate Matter, Ozone and Nitrogen Dioxide, World Health Organization, Bonn, 2003.

Zhang, Q., Streets, D. G., and He, K. B.: Satellite observations of recent power plant construction in Inner Mongolia, China, Geophys. Res. Lett., 36, 5 pp., L15809, doi:10.1029/2009GL038984, 2009a.

Zhang, X., Zhang, P., Zhang, Y., Li, X., and Qiu, H.: The trend, seasonal cycle, and sources of tropospheric NO_2 over China during 1997–2006 based on satellite measurement, Sci. China Ser. D, 50, 1877–1884, doi:10.1007/s11430-007-0141-6, 2007.

Zhang, Y., Dubey, M. K., Olsen, S. C., Zheng, J., and Zhang, R.: Comparisons of WRF/Chem simulations in Mexico City with ground-based RAMA measurements during the 2006-MILAGRO, Atmos. Chem. Phys., 9, 3777–3798, doi:10.5194/acp-9-3777-2009, 2009b.

Zhou, Y., Brunner, D., Hueglin, C., Henne, S., and Staehelin, J.: Changes in OMI tropospheric NO_2 columns over Europe from 2004 to 2009 and the influence of meteorological variability, Atmos. Environ., 46, 482–495, doi:10.1016/j.atmosenv.2011.09.024, 2012.